

Cyclic AMP Potentiates Vascular Endothelial Cadherin-Mediated Cell-Cell Contact To Enhance Endothelial Barrier Function through an Epac-Rap1 Signaling Pathway

Shigetomo Fukuhara,¹ Atsuko Sakurai,¹ Hideto Sano,² Akiko Yamagishi,¹
Satoshi Somekawa,^{1,3} Nobuyuki Takakura,² Yoshihiko Saito,³
Kenji Kangawa,⁴ and Naoki Mochizuki^{1*}

Department of Structural Analysis¹ and Department of Biochemistry,⁴ National Cardiovascular Center Research Institute, Osaka, Department of Stem Cell Biology, Cancer Research Institute, Kanazawa University, Kanazawa,² and First Department of Internal Medicine, Nara Medical University, Nara,³ Japan

Received 2 August 2004/Returned for modification 2 September 2004/Accepted 28 September 2004

Cyclic AMP (cAMP) is a well-known intracellular signaling molecule improving barrier function in vascular endothelial cells. Here, we delineate a novel cAMP-triggered signal that regulates the barrier function. We found that cAMP-elevating reagents, prostacyclin and forskolin, decreased cell permeability and enhanced vascular endothelial (VE) cadherin-dependent cell adhesion. Although the decreased permeability and the increased VE-cadherin-mediated adhesion by prostacyclin and forskolin were insensitive to a specific inhibitor for cAMP-dependent protein kinase, these effects were mimicked by 8-(4-chlorophenylthio)-2'-O-methyladenosine-3', 5'-cyclic monophosphate, a specific activator for Epac, which is a novel cAMP-dependent guanine nucleotide exchange factor for Rap1. Thus, we investigated the effect of Rap1 on permeability and the VE-cadherin-mediated cell adhesion by expressing either constitutive active Rap1 or Rap1GAPII. Activation of Rap1 resulted in a decrease in permeability and enhancement of VE-cadherin-dependent cell adhesion, whereas inactivation of Rap1 had the counter effect. Furthermore, prostacyclin and forskolin induced cortical actin rearrangement in a Rap1-dependent manner. In conclusion, cAMP-Epac-Rap1 signaling promotes decreased cell permeability by enhancing VE-cadherin-mediated adhesion lined by the rearranged cortical actin.

Endothelial cells lining blood vessels regulate endothelial barrier function, which restricts the passage of plasma proteins and circulating cells across the endothelial cells. Endothelial barrier dysfunction results in an increase in vascular permeability, thereby causing edema or inflammatory or metastatic cell infiltration. Inflammatory mediators such as thrombin and histamine induce intercellular gap formation, leading to an increase in endothelial permeability (1, 4). In contrast, angiopoietin 1 and sphingosine-1-phosphate (S1P) stabilize endothelial barrier integrity (17, 18). In addition, cyclic AMP (cAMP), a second messenger downstream of Gs-coupled receptor, improves endothelial cell barrier function (32, 39, 43). Consistently, cAMP-elevating G protein-coupled receptor (GPCR) agonists, adrenomedullin (AM), prostacyclin (PGI₂), prostaglandin E₂ (PGE₂), and β -adrenergic agonists reduce endothelial hyperpermeability induced by inflammatory stimuli (15, 19, 25).

The endothelial cell barrier is structurally organized by adherens junctions (AJ) and tight junctions. Vascular endothelial (VE) cells express both VE-cadherin (also known as cadherin-5 and CD144) and neural (N)-cadherin (9, 33). VE-cadherin constitutes AJ, whereas N-cadherin formed the cell-cell contacts between endothelial cells and endothelial cell-

supporting pericytes. VE-cadherin mediates calcium-dependent, homophilic intercellular adhesion. Its short cytoplasmic tail binds to three armadillo family proteins, β -, γ -, and p120-catenins. β - and γ -catenins associated with α -catenin link the VE-cadherin complex to the actin cytoskeleton and, therefore, strengthen the AJ adhesiveness (9).

Endothelial AJ are dynamic structures, and their adhesive property is finely regulated by several different mechanisms. Tyrosine phosphorylation of VE-cadherin, β -catenin, and p120-catenin correlates with weakened endothelial cell-cell adhesion. VE growth factors and inflammatory mediators such as histamine and thrombin induce tyrosine phosphorylation of AJ components, resulting in the weakened cell-cell contacts and increased endothelial cell permeability (1, 14, 40). In clear contrast, angiopoietin 1, which stabilizes cell-cell contacts, induces dephosphorylation of endothelial cell adhesion molecules, VE-cadherin, and platelet endothelial cell adhesion molecule 1 (17). It has been also reported that S1P induces AJ formation and enhances barrier function through a Rac-dependent cortical actin rearrangement (18). cAMP-dependent protein kinase A (PKA) is suggested to be crucial for cAMP-triggered stabilization of cell-cell contacts and for barrier integrity of endothelial cells (43). However, it has not been clear whether PKA-independent signaling is involved in the regulation of endothelial barrier function.

Rap1, belonging to Ras family GTPase, is involved in the formation and stabilization of AJ in *Drosophila melanogaster* (23). Rap1 becomes the GTP-bound active form by guanine

* Corresponding author. Mailing address: Department of Structural Analysis, National Cardiovascular Center Research Institute, 5-7-1 Fujishirodai, Suita, Osaka 565-8565, Japan. Phone: 81-6-6833-5012, ext. 2508. Fax: 81-6-6835-5461. E-mail: nmochizu@ri.ncvc.go.jp.

nucleotide exchange factor (GEF) and the GDP-bound inactive form by GTPase-activating proteins (GAP), respectively. GEFs for Rap1 include C3G, CalDAG-GEFs, Epacs, and DOCK4 (reviewed in reference 6). DOCK4, which is disrupted in various types of human cancers, regulates the formation of AJ (41). Very recent reports also revealed that Rap1 activity is required for the formation of E-cadherin-based cell-cell contacts (20, 36). These findings prompted us to investigate how Rap1 is activated to stabilize cell-cell contacts and to examine the physiological consequence of stabilized cell-cell contacts by Rap1.

In the present study, we investigated the mechanism by which cAMP-elevating GPCR agonists potentiate endothelial barrier function and restrict cell permeability. We found that increased cAMP triggers Epac-Rap1 signaling to reduce permeability independently of PKA by augmentation of VE-cadherin-mediated cell-cell adhesion.

MATERIALS AND METHODS

Reagents and antibodies. Human recombinant AM was kindly provided by Shionogi & Co. Ltd (31). Materials were purchased as follows: isoproterenol (Iso), PGE₂, PGI₂, thrombin, forskolin (FSK), and 3-isobutyl-1-methylxanthine (IBMX) from Wako Pure Chemical Industries; dibutyl-*c*-AMP (dbcAMP) from Sigma-Aldrich; H89 from Seikagaku Corporation; 8-(4-chlorophenylthio)-2'-*O*-methyladenosine-3',5'-cyclic monophosphate (8-CPT-2'-*O*-Me-cAMP) from Tocris; fluorescein isothiocyanate (FITC)-labeled dextran (molecular weight, 42,000) and purified human immunoglobulin G (IgG) Fc protein from ICN Biologicals; vascular endothelial growth factor (VEGF) from R & D Systems. Anti-Rap1GAPII antibody was developed by immunization of glutathione *S*-transferase (GST)-tagged Rap1GAPII (amino acids 411 to 694 of Rap1GAPII). Other antibodies used here were purchased as follows: anti-VE-cadherin from Chemicon International and Transduction Laboratories; anti- β -catenin from Transduction Laboratories; anti-CREB and anti-phospho-CREB (Ser133) from Cell Signaling Technology; anti-Rap1 from Santa Cruz Biotechnology; anti-cortactin from Upstate Biotechnology, Inc.; rhodamine-phalloidin and Alexa 488-labeled goat anti-mouse IgG from Molecular Probes; horseradish peroxidase-coupled goat anti-mouse and goat anti-rabbit IgG from Amersham Biosciences.

Cell culture and transfection. Human umbilical vein endothelial cells (HUVECs) and human arterial endothelial cells (HAECs) were purchased from Kurabo (Kurashiki, Japan). The cells were maintained in HuMedia-EG2 with a growth additive set as described previously (12) and used for experiments before passages 7 and 10, respectively. HEK293, 293T, and HeLa cells were maintained in Dulbecco's modified Eagle's medium (DMEM; Nissui, Tokyo, Japan) supplemented with 10% fetal bovine serum and antibiotics (100 μ g of streptomycin/ml and 100 U of penicillin/ml). HUVECs and 293T cells were transfected by using Lipofectamine Plus reagent (Invitrogen) and by the calcium-phosphate precipitation technique, respectively.

Plasmids and adenovirus. pcDNA-VE-cad-Ect-Fc-His is a modified vector of pcDNA3.1-Fc-PECAM-1 (a kind gift from W. A. Muller, Cornell University) for producing the secreted form of the extracellular domain of VE-cadherin fused with Fc followed by a six-His tag. A DNA fragment encoding human Epac lacking the cAMP binding domain (amino acids 324 to 881) was amplified by PCR with pMT2SM-HA-Epac (a kind gift from J. L. Bos, Utrecht University, Utrecht, The Netherlands) as a template and ligated into the pCXN2 vector (12). pCXN2-FLAG-Rap1V12-IRES-EGFP expressed both FLAG-tagged Rap1V12 and internal ribosomal entry site (IRES)-driven enhanced green fluorescent protein (EGFP), and pCXN2-Rap1GAPII-IRES-EGFP expressed both FLAG-tagged Rap1GAPII and IRES-driven EGFP. pGL3 control vector was purchased from Promega Corp. Recombinant adenoviruses encoding Rap1GAPII (Ad-RapGAP) and LacZ (Ad-LacZ) were obtained from S. Hattori (The Institute of Medical Science, University of Tokyo) and M. Matsuda (Research Institute for Microbial Disease, Osaka University, Osaka, Japan), respectively. Adenoviruses expressing FLAG-tagged Rap1V12 and IRES-driven EGFP (Ad-Flag-Rap1V12-IRES-EGFP) were produced by using the Adeno-X system according to the manufacturer's protocol (Clontech). Endothelial cells were infected with adenoviruses at the appropriate multiplicities of infection (MOI) as described in the figure legends.

Permeability assay. Permeability across the endothelial cell monolayer was measured by using type I collagen-coated transwell units (6.5-mm diameter, 3.0- μ m-pore-size polycarbonate filter; Corning Costar Corporation). HUVECs plated at 10⁵ cells in each well were cultured for 3 to 4 days before experiments. After serum starvation in medium 199 containing 1% bovine serum albumin (BSA) for 1 h, the cells were treated with the agonists or drugs, as indicated in the figure legends, for 30 min. Permeability was measured by adding 1 mg of FITC-labeled dextran (molecular weight, 42,000)/ml together with or without 2 U of thrombin/ml to the upper chamber. After incubation for 30 min, 50 μ l of sample from the lower compartment was diluted with 300 μ l of phosphate-buffered saline (PBS) and measured for fluorescence at 520 nm when excited at 492 nm with a spectrophotometer F-4500 (Hitachi). HUVECs infected with adenovirus for 24 h after becoming confluent and kept for another 24 h in replaced medium were subjected to a cell permeability assay.

Immunocytochemistry. Monolayer-cultured HUVECs grown on a 35-mm-diameter glass base dish (Asahi Techno Glass) were starved in medium 199 containing 0.5% BSA for 3 h and subsequently incubated with the stimulants indicated in the figure legends for 30 min. After stimulation, the cells were fixed in PBS containing 2% formaldehyde for 30 min at 4°C, washed with PBS, and permeabilized with 0.05% Triton X-100 for 30 min at 4°C. Cells were blocked with PBS containing 4% BSA for 1 h at room temperature (RT) and stained with rhodamine-phalloidin for 20 min, anti-VE-cadherin for 60 min, and anticortactin for 60 min at RT. Protein reacting with antibody was visualized with Alexa 488-labeled goat anti-mouse IgG. Images were recorded with a confocal microscope (BX50WI, Fluoview; Olympus) with a water immersion objective lens (LUMPlanF1 100X1.00W).

VE-cadherin translocation assay and Western blot analysis. HUVECs plated in six-well plates were serum starved in medium 199 containing 1% BSA overnight. The cells were stimulated with PGI₂ and FSK for the indicated time and fractionated with cytoskeleton-stabilizing buffer (10 mM HEPES [pH 7.4], 250 mM sucrose, 150 mM KCl, 1 mM EGTA, 3 mM MgCl₂, 1 \times protease inhibitor cocktail [Roche Diagnostics], 1 mM Na₃VO₄, 0.5% Triton X-100) by centrifugation at 15,000 \times g for 15 min. The Triton X-100-insoluble fraction was subjected to sodium dodecyl sulfate-polyacrylamide gel electrophoresis (SDS-PAGE) followed by transfer to Immobilon-P (Amersham Biosciences) and immunoblotting with the indicated antibodies. Immunocomplexes were visualized by enhanced chemiluminescence detection (Amersham Biosciences) with species-matched peroxidase-conjugated secondary antibodies.

Purification of recombinant VE-cadherin ectodomain-Fc chimeric protein. 293T cells transfected with pcDNA-VE-cad-Ect-Fc-His were cultured in DMEM supplemented with 10% fetal calf serum for 24 h and subsequently kept in replaced medium (DMEM-F21 containing 1% fetal calf serum) for 7 days. VE-cadherin-Fc (VEC-Fc) protein secreted into the medium was collected every 2 days and centrifuged to remove floating cells and debris. VEC-Fc was collected on ProBond resin (Invitrogen) by gentle agitation overnight at 4°C. VEC-Fc protein bound to the beads was eluted with 500 mM imidazole, concentrated with Amicon Centriplus 30 (Millipore), and buffer exchanged into PBS containing 2 mM CaCl₂ and 2 mM MgCl₂ (PBS-Ca/Mg) by dialysis.

Cell adhesion assay. Twenty-four-well tissue culture plates were coated with 10 μ g of VEC-Fc or Fc protein/ml in PBS-Ca/Mg at 4°C overnight. After washing with PBS-Ca/Mg, the plates were blocked with 1% heat-inactivated BSA in PBS (heat inactivated at 85°C for 12 min) for 1 h at RT. To examine cell adhesion to the VEC-Fc- or Fc-coated dish, cells were suspended in 0.5% BSA-containing medium 199 and incubated for 30 min at 37°C. Cells (1.5 \times 10⁵) were plated on each VEC-Fc- or Fc-coated well in the presence or absence of agonists, drugs, and 5 mM EGTA and adhered to the dish at 37°C for the indicated time. To analyze cell adhesion to a collagen-covered surface, cells were plated onto a collagen-coated six-well plate (Iwaki) and adhered to the dish in the presence or absence of 5 mM EGTA. After washing with PBS-Ca/Mg four times to remove nonadherent cells, adherent cells and input cells were quantified by measuring endogenous alkaline phosphatase activity as described elsewhere (35). Briefly, the cells were lysed in a buffer containing 100 mM Tris-citrate (pH 6.5) and 0.25% Triton X-100, and alkaline phosphatase activity in the lysate was measured by using the AttoPhos AP fluorescent substrate system (Promega Corp.). To examine the effects of Rap1V12, Epac Δ cAMP, and Rap1GAPII, HUVECs were transfected with plasmids encoding either Rap1V12, Epac Δ cAMP, or Rap1GAPII together with the luciferase reporter construct (pGL3 control vector). The adhesion of cells expressing Rap1V12, Epac Δ cAMP, or Rap1GAPII to the VEC-Fc-coated dish was normalized by measuring the luciferase activity of the cells and input cells (16).

Detection of GTP-bound form of Rap1. Rap1 activity was assessed by a modified Bos's method as described previously (34). Briefly, HUVECs starved in medium 199 containing 1% BSA overnight were stimulated with the indicated

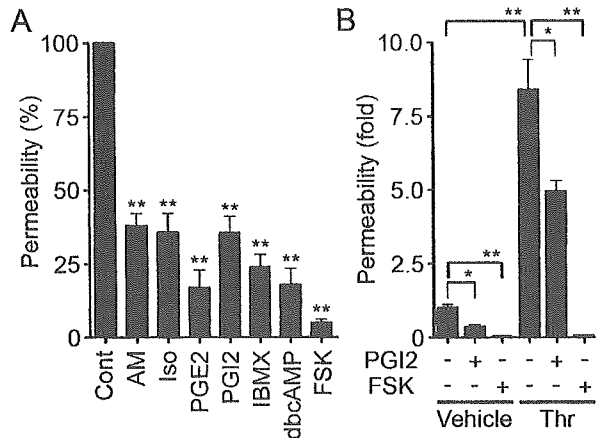


FIG. 1. cAMP enhances barrier function of monolayer VE cells. (A) Vascular permeability, reflecting barrier function, was analyzed by measuring the fluorescence of FITC-labeled dextran across the monolayer-cultured HUVECs as described in Materials and Methods. HUVECs grown on transwell filters were incubated with control (Cont), 0.1 μ M AM, 200 μ M Iso, 200-ng/ml PGE2, 10- μ g/ml PGI2, 1 mM IBMX, 1 mM dbcAMP, and 10 μ M FSK for 30 min. Average permeability \pm standard deviation is expressed as a percentage compared to the control. (B) The effects of PGI2 and FSK on vascular permeability were quantified in the presence (+) or absence (-) (Vehicle) of 2 U of thrombin (Thr)/ml. Average permeability \pm standard deviation is expressed as the increase relative to that observed in unstimulated HUVECs in the vehicle. Data shown are the results from at least three independent experiments. Significant differences from the control (A) or between two groups (B) determined by Student's *t* test are indicated by a single asterisk ($P < 0.05$) or double asterisks ($P < 0.01$).

agonists and drugs and lysed at 4°C in a pull-down lysis buffer (20 mM Tris-HCl [pH 7.5], 100 mM NaCl, 10 mM MgCl₂, 1% Triton X-100, 1 mM EGTA, 1 mM dithiothreitol, 1 mM Na₃VO₄, 1× protease inhibitor cocktail). GTP-bound Rap1 was collected on the GST-Rap1 binding domain of RasGDS precoupled to glutathione-Sepharose beads and subjected to SDS-PAGE followed by immunoblotting with anti-Rap1.

In vivo permeability assay. In vivo permeability was quantified by a modified Miles assay as described previously (29). In brief, ICR mice (Japan SLC, Inc.) shaved 3 days before experiments were lightly anesthetized and intravenously injected with 150 μ l of 1% Evans blue dye solution (in saline) passed through a 0.22- μ m-pore-size filter. Fifteen minutes later, 20 μ l of PBS, VEGF (50 μ g/ml), and/or 8-CPT-2'-O-Me-cAMP (1 mM) were applied by intradermal injections with a 30-gauge needle. The sites of intradermal injection were photographed 60 min after the injection, carefully dissected, and weighed. To quantify the vascular permeability, extravasated blue dye was eluted from the dissected skin with formamide at 56°C, and optical density was measured by spectrophotometry at 620 nm.

RESULTS

cAMP enhances the barrier property of monolayer-cultured endothelial cell. To evaluate the barrier function, we examined the permeability of FITC-labeled dextran across monolayer HUVECs. Expectedly, AM, Iso, PGE2, and PGI2 reduced basal endothelial permeability in HUVECs (Fig. 1A). PGI2 also reduced thrombin-induced vascular permeability (Fig. 1B). Other cAMP-elevating bio-ligands similarly reduced thrombin-induced permeability (data not shown). The bio-ligands for cAMP-elevating GPCR that we used in this study indeed increased cAMP in HUVECs (data not shown). Furthermore, IBMX (an inhibitor for phosphodiesterase), dbcAMP (a membrane-permeable cAMP analogue), and FSK

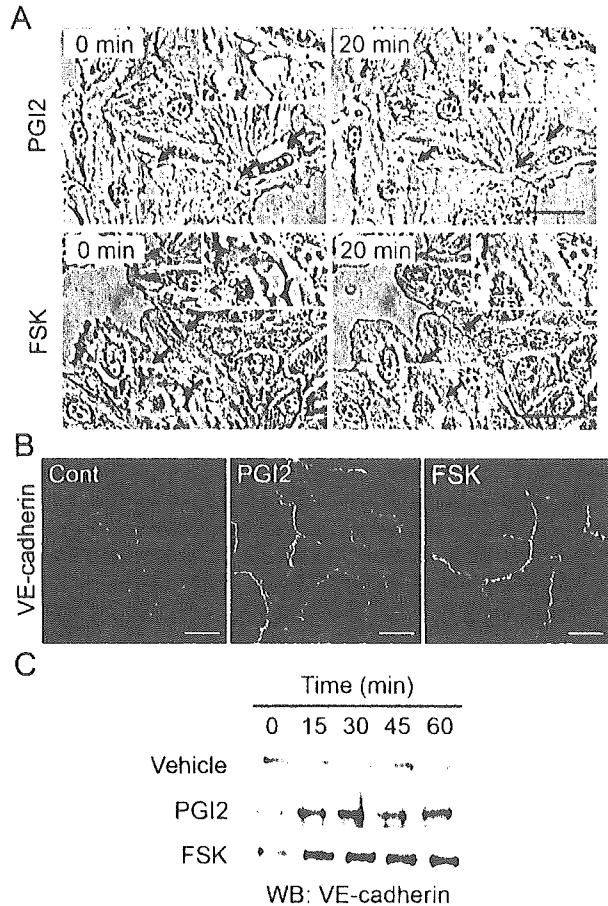


FIG. 2. cAMP induces AJ formation. (A) HUVECs cultured on a glass base dish were stimulated with 10 μ g of PGI2/ml (upper panels) or with 10 μ M FSK (lower panels) for 20 min and shown as phase-contrast images. Left and right panels show the cells before and after stimulation, respectively. The arrows indicate the sites of cell-cell contacts induced by PGI2 and FSK. The area boxed by the white broken line is enlarged in the right top of the panels. Bars, 50 μ m. (B) Subconfluent HUVECs stimulated with vehicle (Cont), 10- μ g/ml PGI2, and 10 μ M FSK for 45 min were fixed, stained with anti-VE-cadherin antibody, and visualized with Alexa 488-conjugated secondary antibody through a confocal microscope (BX50WI; Olympus). Note that VE-cadherin (green) was accumulated at the cell-cell contact upon PGI2 and FSK stimulation. Bars, 50 μ m. (C) Translocation of VE-cadherin was assessed by Triton X-100 solubility. HUVECs were stimulated with vehicle (top), 10- μ g/ml PGI2 (middle), and 10 μ M FSK (bottom) for the time indicated at the top and fractionated with cytoskeleton-stabilizing buffer as described in Materials and Methods. The Triton X-100-insoluble fraction was subjected to SDS-PAGE followed by Western blot analysis (WB) with anti-VE-cadherin.

(an adenylyl cyclase activator) resulted in a reduction of both basal and thrombin-induced endothelial permeability (Fig. 1; data not shown).

cAMP potentiates formation of AJ. Endothelial barrier function is largely dependent upon endothelial cell junctions. To investigate how cAMP affects AJ formation, we examined AJ organization by immunostaining with anti-VE-cadherin before and after stimulation. When subconfluent HUVECs with intercellular gaps were stimulated with PGI2 or FSK, the cells extended the plasma membrane and established cell-cell contacts with neighboring cells (Fig. 2A). Similar results were

obtained with AM and PGE2 (data not shown). Stimulation of HUVECs with PGI2 and FSK dramatically enhanced accumulation of VE-cadherin at cell-cell contacts (Fig. 2B).

The maturation of AJ requires homophilic binding of intercellular VE-cadherins and tight anchoring to the actin cytoskeleton via the cytoplasmic region through catenins. VE-cadherin anchored to the actin cytoskeleton is detected in detergent-insoluble fractions of cell lysates (26). We found an increase in VE-cadherin in the Triton X-100-insoluble fraction after stimulation with PGI2 or FSK (Fig. 2C). These results suggest that cAMP-elevating GPCR agonists potentiate AJ formation, which results in a cAMP-induced decrease in permeability.

cAMP promotes VE-cadherin-dependent endothelial cell adhesion. VE-cadherin is required for AJ formation (9). To test the involvement of a homophilic interaction of VE-cadherin in cAMP-enhanced AJ formation, we directly examined VE-cadherin-mediated cell adhesion. To mimic the VE-cadherin-dependent cell adhesion, we used VEC-Fc chimeric protein, which consisted of the extracellular domain of VE-cadherin fused to the Fc portion of immunoglobulin. HUVECs were plated onto VEC-Fc-coated dishes and time-lapse imaged. Cells attached within 5 min to the VEC-Fc-coated dish, subsequently spread, and exhibited a typical fried-egg morphology characterized by a large circular lamellipodium (Fig. 3A). No cells attached to the Fc-coated dish (Fig. 3B and C). Since cadherin-dependent cell adhesion requires Ca^{2+} , we examined the effect of Ca^{2+} chelation on cell adhesion to VEC-Fc-coated dishes. Cell adhesion to VEC-Fc-coated dishes was completely abolished by chelating extracellular Ca^{2+} , although cell attachment to the collagen-coated dish was unaffected (Fig. 3C and D). Basal and FSK-augmented cell adhesion to VEC-Fc-coated dishes was inhibited by EGTA (Fig. 3C). Both HUVECs and HAECs expressing VE-cadherin adhered to the VEC-Fc-coated dish (Fig. 3E). In clear contrast, HeLa and HEK293 cells, which express N-cadherin, but not VE-cadherin (20, 42), did not adhere to the VEC-Fc-coated dish, although these cells could attach to the collagen-coated dish (Fig. 3E; data not shown). Collectively, these results indicate that endothelial cell adhesion to the VEC-Fc-coated dish depends upon the homophilic ligation of VE-cadherin.

We proceeded to investigate the effect of cAMP-elevating GPCR agonists on VE-cadherin-mediated cell adhesion. The adhesion of HUVECs plated in the presence of PGI2 or FSK was evaluated by the alkaline phosphatase activity of remaining cells after washing. PGI2 enhanced adhesion of HUVECs to the VEC-Fc-coated dish in a concentration-dependent manner (Fig. 4A) and in a time-dependent manner (Fig. 4B). In a time course analysis, we noticed that enhanced adhesion was observed 7 min after the plating (Fig. 4B). Other cAMP-elevating GPCR agonists, including AM, Iso, and PGE2, potentiated VE-cadherin-dependent cell adhesion (Fig. 4C). In addition, similarly enhanced cell adhesion to the VEC-Fc-coated dish was also observed in the cells treated with cAMP-elevating drugs such as IBMX, dbcAMP, and FSK (Fig. 4F). Like PGI2, the effect of FSK on cell adhesion to the VEC-Fc-coated dish was concentration dependent and time dependent (Fig. 4D and E). This cAMP-induced cell adhesion to the VEC-Fc-coated dish depends on the enhanced homophilic ligation of VE-cadherin because FSK did not augment endothelial adhe-

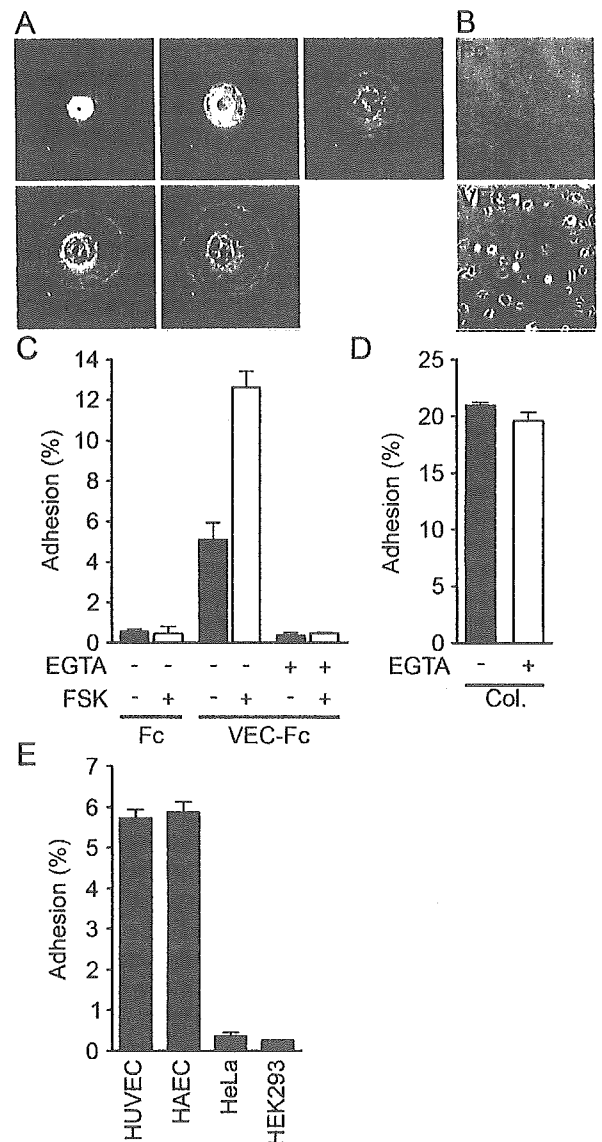


FIG. 3. Endothelial cells adhere to a VEC-Fc-coated dish through homophilic ligation of VE-cadherin. (A) HUVECs were plated onto the VEC-Fc-coated dish and time-lapse imaged at the time points (in minutes) indicated on the panels. Bar, 20 μ M. (B) HUVECs were plated on the Fc-coated dish (top panel) or the VEC-Fc-coated dish (bottom panel) for 1 h and phase-contrast imaged after removal of nonadherent cells by washing with PBS-Ca/Mg. (C) HUVECs were plated onto either an Fc- or VEC-Fc-coated dish in the absence (-) or presence (+) of 5 mM EGTA and 10 μ M FSK for 7 min. Cell adhesion was quantified as described in Materials and Methods. (D) Adhesion of HUVECs to a collagen-coated dish in the presence or absence of 5 mM EGTA was analyzed by a method similar to that described for panel C. (E) Adhesion of HUVECs, HAECs, and HeLa and HEK293 cells to the VEC-Fc-coated dish was examined as described in the legend for panel C. Cells adhering to the dishes of total input cells (percentage) is expressed as the mean \pm standard deviation by measuring alkaline phosphatase activity of adherent cells divided by that of total input cells. Representative results from three independent experiments were shown in all panels.

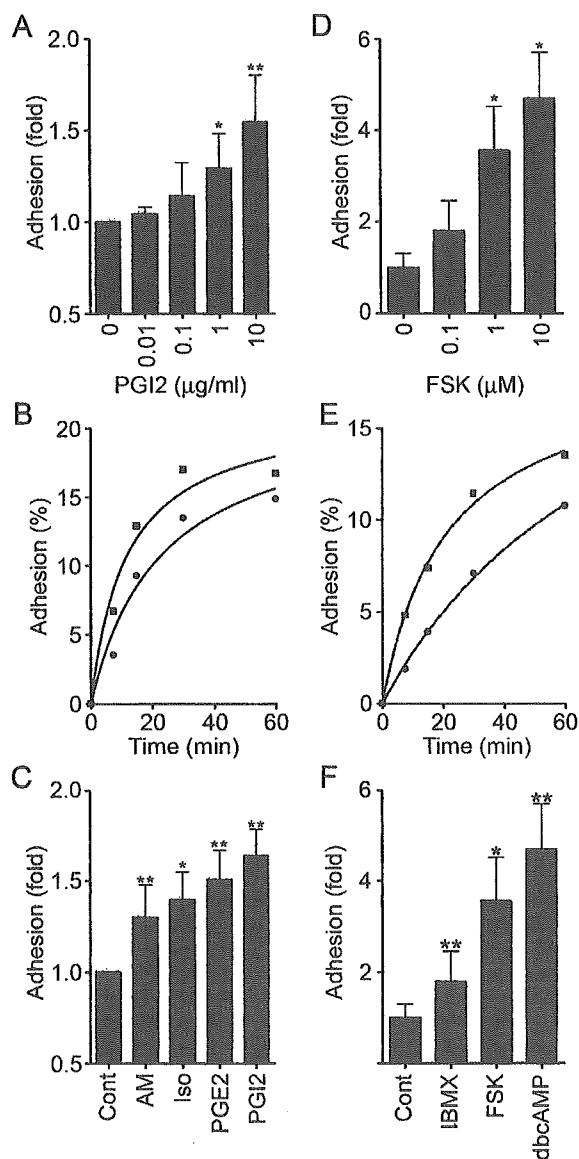


FIG. 4. cAMP potentiates VE-cadherin-dependent cell adhesion. (A) HUVECs were plated onto a VEC-Fc-coated dish in the presence of PGI2 at the concentrations indicated at the bottom for 7 min. Cell adhesion was quantified as described in Materials and Methods. Mean adhesion activity \pm standard deviation is expressed as the increase compared with that observed in unstimulated cells. (B) HUVECs were plated onto the VEC-Fc-coated dish in the absence (circle) or presence (square) of 10- μ g/ml PGI2 for the time indicated at the bottom. The percent adhesion was calculated by measuring the alkaline phosphatase activity of adherent cells divided by that of total input cells. (C) HUVECs stimulated with cAMP-elevating ligands similar to that described in the legend to panel A were assessed for adhesion activity. The concentration of stimulants was the same as described in the legend to Fig. 1A. (D) The effect of FSK on cell adhesion was analyzed by a method similar to that described for panel A, except that cells were preincubated for 10 min before plating. (E) The effect of 10 μ M FSK on time-dependent adhesion was analyzed as described in the legend to panel B, except that cells were preincubated for 10 min before plating. (F) HUVECs stimulated with the reagent indicated at the same concentration used as described in the legend to Fig. 1A were analyzed for cell adhesion by a method similar to that described for panel D. Data are expressed as means \pm standard deviations of the results from three independent experiments in panels A, C, D, and F. Representative results from three independent experiments were

shown to the Fc-coated dish or attachment to the VEC-Fc-coated dish in the absence of extracellular Ca^{2+} (Fig. 3C). These results indicate that cAMP potentiates VE-cadherin-dependent cell adhesion.

cAMP augments endothelial barrier function in a PKA-independent manner. PKA is suggested to be involved in cAMP-enhanced endothelial barrier function (43). Thus, we investigated the involvement of PKA in the regulation of endothelial barrier integrity by PGI2 and FSK. Unexpectedly, PGI2- and FSK-induced reduction of endothelial permeability was insensitive to a specific PKA inhibitor, H89 (7) (Fig. 5A and B). The reduction of thrombin-increased permeability by FSK was also unaffected by H89 (Fig. 5C). Consistently, H89 did not affect VE-cadherin-mediated cell adhesion enhancement by PGI2 and FSK (Fig. 5D and E). To confirm that H89 worked in HUVECs, we examined FSK-induced phosphorylation of CREB, a direct PKA substrate (38). Phosphorylation of CREB upon FSK stimulation was significantly inhibited by H89, indicating the effectiveness of this inhibitor in HUVECs (Fig. 5F). Therefore, these results apparently suggest a novel PKA-independent signaling pathway involved in cAMP-induced endothelial barrier function.

cAMP induces Rap1 activation. Besides PKA, Epac (cAMP-GEF) was identified as a novel cAMP target and a Rap1-specific GEF (5, 21). We therefore hypothesized that cAMP-activated Epac-Rap1 signaling is involved in the enhancement of VE-cadherin-dependent cell adhesion and endothelial barrier function. To address this possibility, we tested whether cAMP-elevating GPCR agonists induce Rap1 activation in HUVECs. Rap1 activity was determined by a pull-down assay by using a GST fusion protein of Rap1-binding domain of RalGDS according to the Bos's method. Bio-ligands for cAMP-elevating GPCR activated Rap1 (Fig. 6A). PGI2 rapidly induced Rap1 activation, which peaked at 1 to 5 min after the stimulation and then declined to the basal level by 10 min (Fig. 6C). A second wave of Rap1 activation was also observed 15 to 45 min after the stimulation (Fig. 6C). PGI2-induced Rap1 activation occurred in a concentration-dependent manner (Fig. 6B), which was associated with enhancement of VE-cadherin-dependent cell adhesion (Fig. 4A). Similarly, dbcAMP, FSK, and IBMX activated Rap1 (Fig. 6D). FSK-induced Rap1 activation reached a maximal level 2 to 5 min after the stimulation, and the level was sustained for up to 15 to 30 min (Fig. 6E). Collectively, these findings indicate that cAMP induces Rap1 activation in endothelial cells.

Specific activation of Epac reduces endothelial permeability and enhances VE-cadherin-dependent cell adhesion. To test whether the activation of endogenous Epac is sufficient to reduce endothelial permeability and to induce VE-cadherin-dependent cell adhesion, we used a recently developed cAMP analog, 8-CPT-2'-O-Me-cAMP, which specifically activates Epac without affecting PKA activity (13). As expected, 8-CPT-2'-O-Me-cAMP induced Rap1 activation in HUVECs (Fig. 7A), indicating that Epac is expressed in endothelial cells.

shown in panels B and E. A significant difference from the control determined by Student's *t* test is indicated with a single asterisk ($P < 0.05$) or double asterisks ($P < 0.01$).

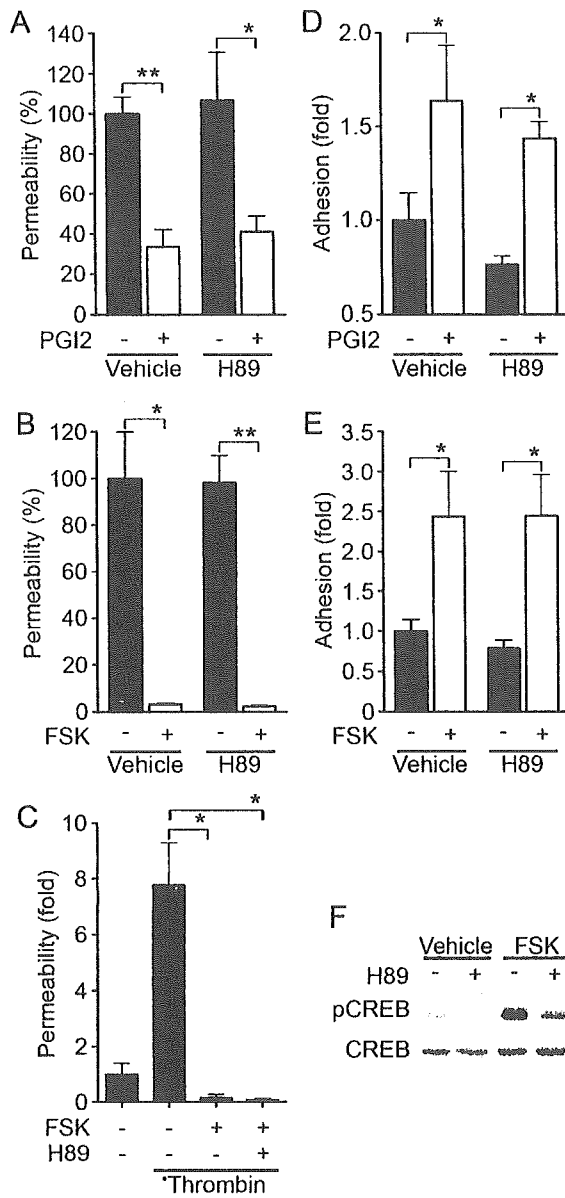


FIG. 5. cAMP-enhanced VE-cadherin-dependent cell adhesion and endothelial barrier function does not depend upon PKA. (A) Permeability across monolayer HUVECs grown on transwell filters were assessed by measuring FITC-labeled dextran as described in the legend to Fig. 1A. The effect of 10- μ g/ml PGI2 on cell permeability without pretreatment (Vehicle) or with pretreatment with 5 μ M H89, a specific PKA inhibitor, for 10 min is indicated as the percent permeability compared to that observed in untreated cells. +, present; -, absent. (B) The effect of 10 μ M FSK on cell permeability without pretreatment (Vehicle) and with pretreatment with H89 was assessed similar to that described for panel A. (C) The effect of pretreatment of HUVECs with 5 μ M H89 on FSK-induced reduction of 2-U/ml thrombin-induced permeability was analyzed. Permeability indicates the increase relative to that observed in untreated cells. (D) HUVECs untreated or pretreated with H89 for 10 min prior to stimulation with 10- μ g/ml PGI2 were analyzed for cell adhesion as described in the legend to Fig. 4A. (E) HUVECs untreated or pretreated with H89 for 10 min prior to stimulation with 10 μ M FSK were analyzed for cell adhesion as described in the legend to Fig. 4D. For panels A to E, data are expressed as means \pm standard deviations of the results from triplicate samples. Similar results were obtained in at least three independent experiments. Significant differences between two groups determined

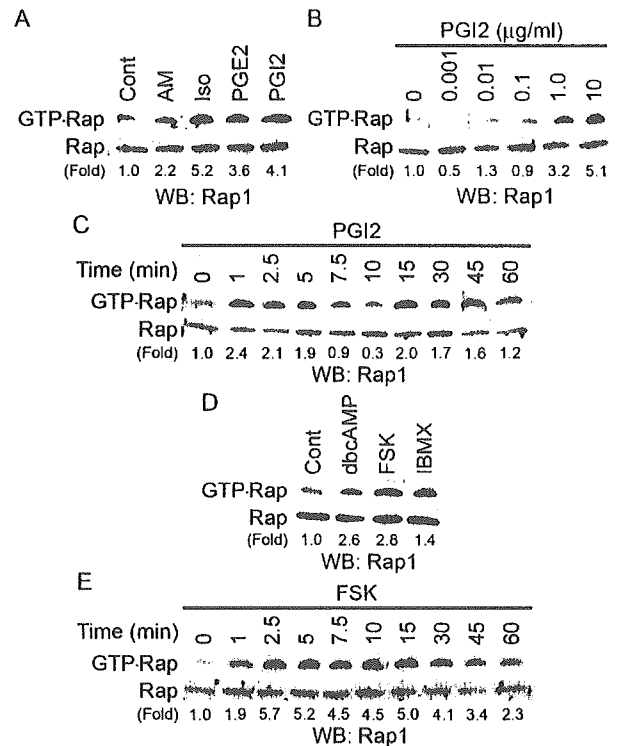


FIG. 6. cAMP induces Rap1 activation. (A) Serum-starved HUVECs kept in medium 199 containing 1% BSA overnight were stimulated with cAMP-elevating agonists for 2.5 min as indicated at the top and at the concentrations described in the legend to Fig. 1A. GTP-bound Rap1 was detected by pull-down assay as described in Materials and Methods. Activation indicates the ratio of the poststimulation GTP-Rap1 intensity of total Rap1 intensity to the prestimulation GTP-Rap1 intensity of total Rap1 intensity. (B) Rap1 activation was analyzed by detecting GTP-bound Rap1 with lysates from HUVECs stimulated with PGI2 for 2.5 min at the different concentrations indicated at the top. (C) Rap1 activation was analyzed by detecting GTP-bound Rap1 with lysates from cells stimulated with 10- μ g/ml PGI2 for the time period indicated at the top. (D) Serum-starved HUVECs similar to those described in the legend to panel A were stimulated with the reagents indicated at the top for 10 min at the same concentrations described in the legend to Fig. 1A. Rap1 activation was assessed by a method similar to that described for panel A. (E) The effect of 10 μ M FSK on time-dependent Rap1 activity was examined as described for panel C. Representative results from at least three independent experiments are shown for all panels.

8-CPT-2'-O-Me-cAMP dramatically reduced basal endothelial permeability, as did FSK and dbcAMP (Fig. 7B). Thrombin-induced permeability was also inhibited by 8-CPT-2'-O-Me-cAMP (Fig. 7C). Furthermore, we examined the effect of 8-CPT-2'-O-Me-cAMP on in vivo vascular permeability. VEGF-induced vascular permeability was completely blocked by coinjection of 8-CPT-2'-O-Me-cAMP (Fig. 7D). In addition, adhesion

by Student's *t* test are indicated by a single asterisk ($P < 0.05$) or double asterisks ($P < 0.01$). (F) HUVECs serum starved in 1% BSA-containing medium 199 for 6 h, followed by pretreatment with (+) or without (-) 5 μ M H89 for 10 min, were stimulated with vehicle and 10 μ M FSK for 10 min. Phosphorylation of CREB was assessed by Western blot analysis with anti-CREB (CREB) and anti-phospho-CREB-specific (pCREB) antibodies.

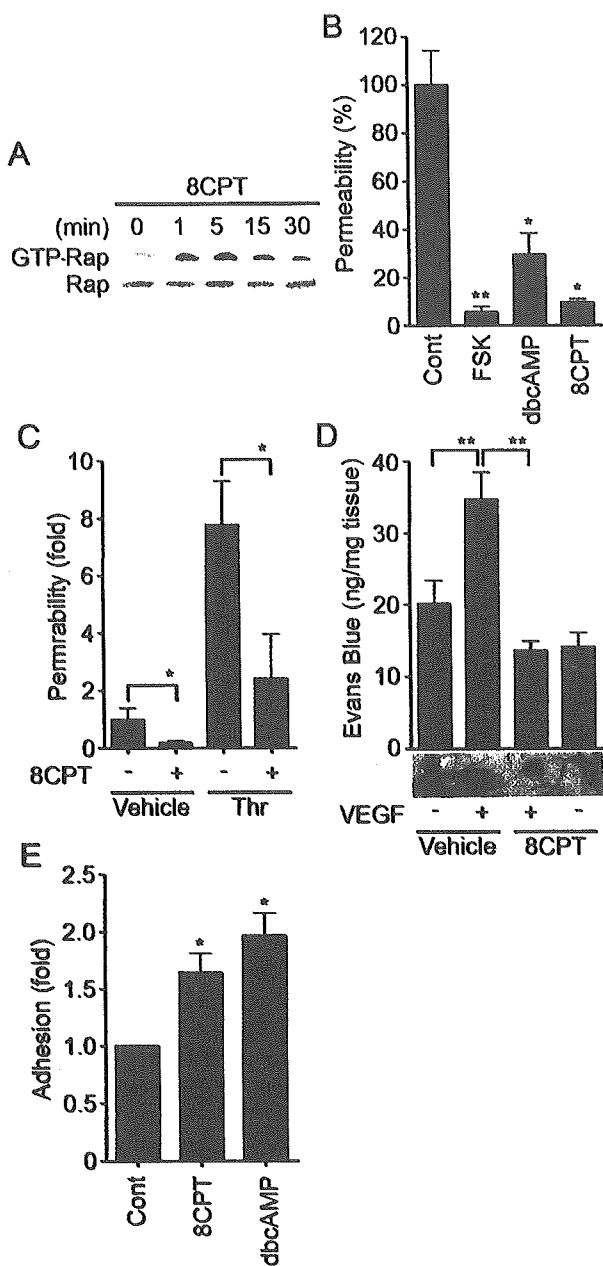


FIG. 7. Activation of Epac is sufficient to enhance VE-cadherin-dependent cell adhesion and endothelial barrier function. (A) Serum-starved HUVECs in medium 199 containing 1% BSA were stimulated with 0.2 mM 8-CPT-2'-O-Me-cAMP (8CPT) for the indicated time. Rap1 activity was determined as described in the legend to Fig. 6A. The result is a representative from three independent experiments. (B) Permeability of cells treated with the reagents as indicated on the bottom for 30 min was analyzed as described in the legend to Fig. 1A. (C) The effect of 0.2 mM 8CPT-2'-O-Me-cAMP on 2-U/ml thrombin-induced permeability was analyzed as described in the legend to Fig. 1B. (D) Effect of 8CPT-2'-O-Me-cAMP on VEGF-induced permeability was assessed by intradermal Miles assay as described in Materials and Methods. Amounts of extravasation of Evans blue in mouse dermal skin were measured 60 min after intradermal injection of vehicle and VEGF together with (+) or without (-) 8CPT. Mean leakage \pm standard deviation of the results from 6 mice per group is expressed as nanograms of weight of extravasated Evans blue per milligram of weight of dermal skin. A photograph on the bottom shows leakage of Evans blue in dermal skin. (E) HUVEC adhesion to the VEC-Fc-coated dish in the presence of 0.2 mM 8CPT and 1 mM dbcAMP for

of HUVECs to the VEC-Fc-coated dish was significantly enhanced by 8-CPT-2'-O-Me-cAMP (Fig. 7E). Hence, Epac activation is sufficient to enhance VE-cadherin-dependent cell adhesion and to augment endothelial barrier function in vitro and in vivo.

Rap1 activation is essential for VE-cadherin-dependent cell adhesion and endothelial barrier function. We next proceeded to investigate the role of Rap1 in VE-cadherin-dependent cell adhesion and endothelial barrier function. To examine the effect of Rap1 on cell permeability and VE-cadherin-mediated cell adhesion, we inactivated endogenous Rap1 by adenovirus-expressing Rap1GAPII (Ad-RapGAP), which specifically catalyzes the hydrolysis of GTP to GDP on Rap1 (30). As shown in Fig. 8A, endogenous Rap1 activity was almost completely suppressed by the expression of increasing amounts of Rap1GAPII in HUVECs. This Rap1 inactivation paralleled the increase in basal permeability (Fig. 8B) and the inhibition of cell adhesion to the VEC-Fc-coated dish (Fig. 8D). In contrast, a constitutively active Rap1, Rap1V12, reduced both basal and thrombin-increased cell permeability (Fig. 8C). VE-cadherin-mediated cell adhesion was also enhanced by Rap1V12 and Epac Δ cAMP, a constitutively active mutant of Epac (Fig. 8D). Taken together, these results indicate that Rap1 activation is required for VE-cadherin-mediated cell adhesion and endothelial barrier function.

cAMP enhances VE-cadherin-dependent cell adhesion and endothelial barrier function by activating Rap1. To test the requirement for Rap1 in endothelial barrier enhancement by cAMP-elevating GPCR agonists, we infected HUVECs with Ad-RapGAP and examined the effect of inactivation of Rap1 on PGI₂- and FSK-induced reduction of cell permeability. Although basal endothelial permeability was reduced by PGI₂ and FSK (Fig. 9A and B), overexpression of Rap1GAPII increased not only basal but also PGI₂- and FSK-reduced endothelial permeability, indicating the requirement of Rap1 activity for PGI₂- and FSK-induced barrier enhancement. We also investigated the involvement of Rap1 in PGI₂- and FSK-induced VE-cadherin-dependent cell adhesion. PGI₂ and FSK augmented VE-cadherin-dependent cell adhesion of HUVECs infected with control adenovirus (Ad-LacZ); however, their effects were dramatically suppressed by overexpression of Rap1GAPII (Fig. 9C and D). These data demonstrate that cAMP enhances VE-cadherin-dependent cell adhesion and endothelial barrier functions by activating Rap1.

cAMP induces endothelial cortical actin rearrangement in a Rap1-dependent manner. Endothelial barrier function is largely dependent upon the actin cytoskeleton supporting junctional adhesion molecules (10). Thus, we examined the effect of cAMP on cortical actin polymerization and assembly of polymerized actin in a monolayer of endothelial cells. Cortactin, an actin-binding protein, is known to be implicated in cortical actin rearrangement (8) and suggested to regulate S1P-induced endothelial barrier enhancement (11). PGI₂,

7 min was analyzed as described in the legend to Fig. 4F. In panels B, C, and E, data are expressed as means \pm standard deviations of the results from triplicate samples. A significant difference from the control in panels B and E or between two groups in panels C and D was determined by Student's *t* test and indicated by a single asterisk ($P < 0.05$) or double asterisks ($P < 0.01$).

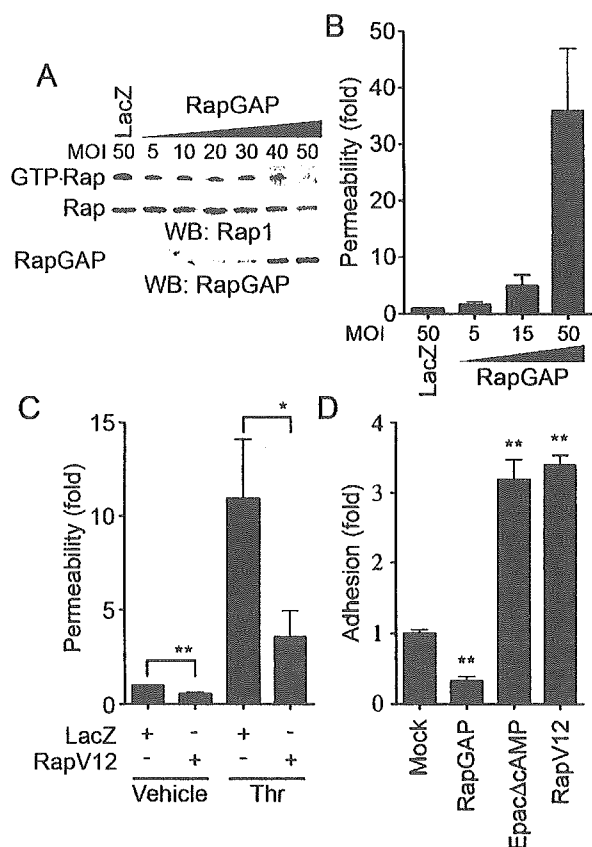


FIG. 8. Rap1 plays a critical role in VE-cadherin-dependent cell adhesion and endothelial barrier function. (A) Rap1 inactivation was assessed by detecting GTP-Rap1 in HUVECs infected with different MOI of adenovirus-expressing Rap1GAPII (RapGAP) as indicated at the top. An adenovirus-expressing LacZ at an MOI of 50 was used as a control. GTP-bound Rap1 (GTP-Rap) was detected by pull-down assay as described in Materials and Methods. Rap1 (Rap) and Rap1GAPII (RapGAP) expression were examined by Western blot analysis. (B) The permeability of FITC-dextran across HUVECs infected with adenovirus as indicated at the bottom was analyzed as described in Materials and Methods. Data are the means \pm standard deviations of the results from three independent experiments and are expressed as increases relative to those of LacZ-infected cells. (C) Monolayer HUVECs infected with either an adenovirus-expressing LacZ or that expressing Rap1V12 at an MOI of 50 for 24 h were medium changed and cultured for another 24 h. The permeability of cells upon 2-U/ml thrombin stimulation (Thr) after starvation for 1 h was analyzed as described in the legend to Fig. 1B. Data are the means \pm standard deviations of the results from five independent experiments and are expressed as inductions relative to those of untreated HUVECs infected with the LacZ-expressing virus. (D) HUVECs were transfected with either empty vector (Mock), plasmids expressing Rap1GAPII (RapGAP), EpacΔcAMP, or Rap1V12 together with the luciferase reporter construct. Transfected cells were plated on the VEC-Fc-coated dish and allowed to adhere for 15 min. Cell adhesion was analyzed as described in Materials and Methods. Data are expressed as increases compared to those of mock-transfected cells. The results indicate the means \pm standard deviations of the results from triplicate samples. Similar results were obtained in three independent experiments. Significant differences between two groups in panel C or from the control in panel D are determined by Student's *t* test and are indicated by a single asterisk ($P < 0.05$) or double asterisks ($P < 0.01$).

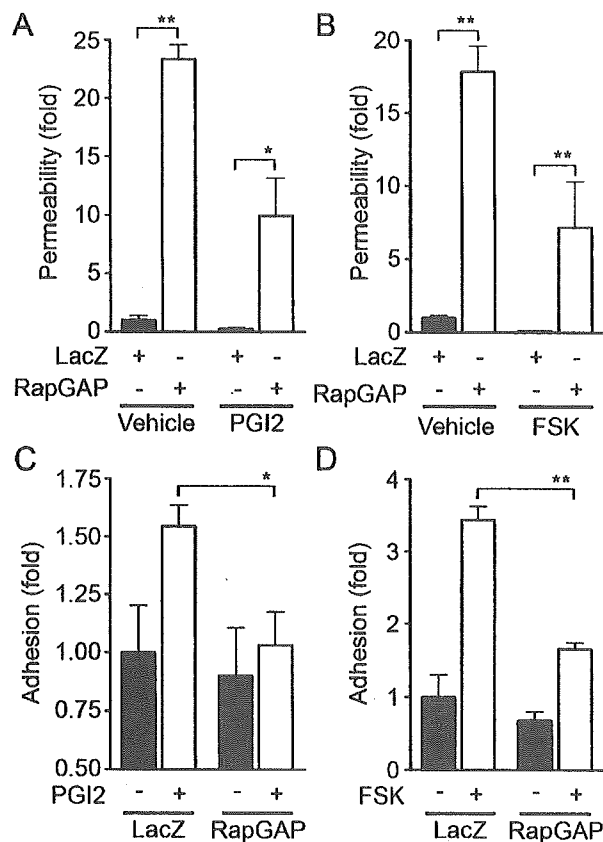


FIG. 9. Inactivation of Rap1 reduces PGI2- and FSK-induced barrier function and VE-cadherin-mediated cell adhesion. (A) Monolayer-cultured HUVECs grown on transwell filters were infected with either LacZ-expressing adenovirus (Ad-LacZ) or Rap1GAPII-expressing virus (Ad-RapGAP) at an MOI of 40 for 24 h. Medium was replaced with fresh medium after infection. Cells were cultured for an additional 24 h and treated with 10 μ g of PGI2/ml for 30 min after serum starvation for 1 h. Permeability was analyzed as described in Materials and Methods. (B) The effect of 10 μ M FSK on permeability in HUVECs infected with Ad-RapGAP was similarly analyzed. (C) HUVECs were infected with either Ad-LacZ or Ad-RapGAP at an MOI of 40 for 24 h. HUVECs resuspended in medium 199 with 0.5% BSA were plated onto VEC-Fc-coated dishes in the presence (+) or absence (-) of 10 μ g of PGI2/ml for 7 min. Cell adhesion activity was quantified as described in the legend to Fig. 4A. (D) The effect of FSK on adhesion of HUVECs infected with Ad-RapGAP was analyzed similarly to that described for panel C. Resuspended HUVECs were preincubated with 10 μ M FSK for 10 min before plating. Significant differences between two groups determined by Student's *t* test are indicated by a single asterisk ($P < 0.05$) or double asterisks ($P < 0.01$).

FSK, and 8-CPT-2'-O-Me-cAMP dramatically induced accumulation of polymerized actin and cortactin at cell-cell contacts (Fig. 10A). To explore the involvement of Rap1 in cAMP-mediated cortical actin rearrangement, an expression vector encoding Rap1GAPII was introduced into endothelial cells. FSK enhanced actin polymerization at cell-cell contacts in cells transfected with control vector encoding EGFP, whereas it did not in cells expressing Rap1GAPII (Fig. 10B). Cytochalasin D, an actin-depolymerizing agent, attenuated FSK-induced barrier enhancement (Fig. 10C) and inhibited FSK-induced VE-cadherin-dependent cell adhesion (Fig. 10D). These results suggest that the cortical actin rearrangement promoted by

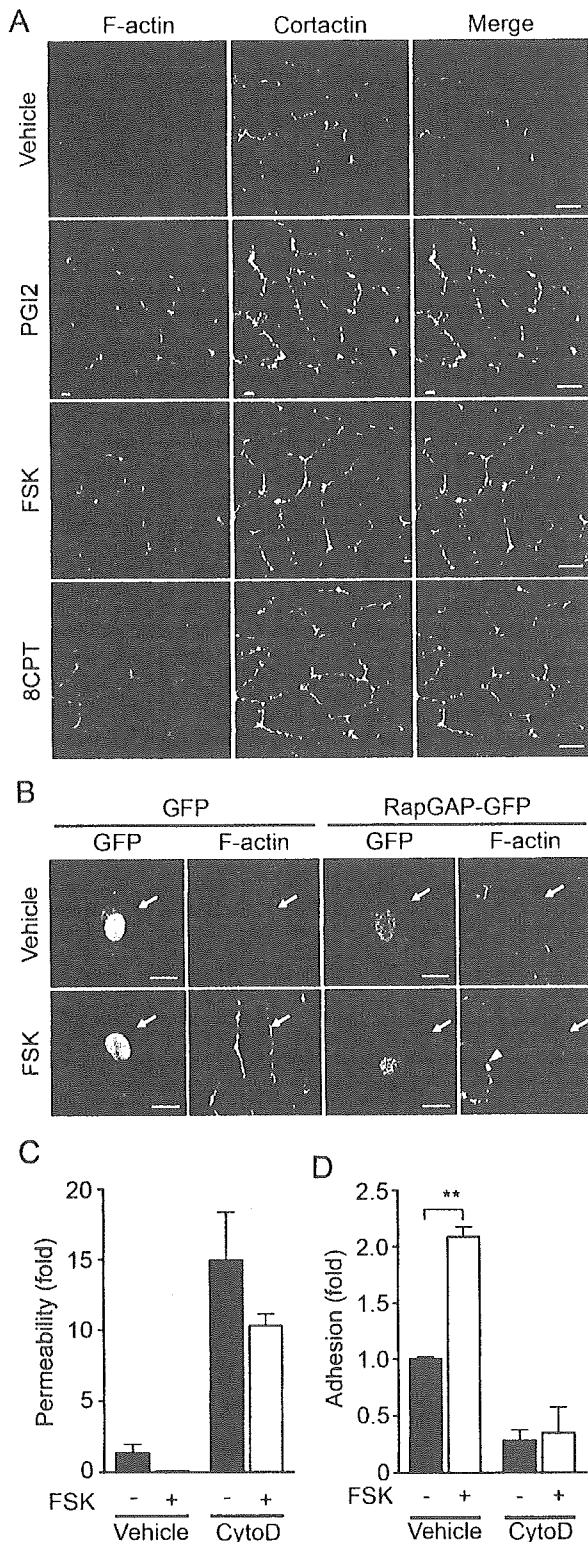


FIG. 10. cAMP induces cortical actin rearrangement in a Rap1-dependent manner. (A) Monolayer-cultured HUVECs starved in 0.5% BSA-containing medium 199 for 3 h were stimulated with vehicle (top row), 10- μ g/ml PGI₂ (second row), 10 μ M FSK (third row), and 0.2 mM 8-CPT-2'-O-Me-cAMP (8CPT) (bottom row) for 30 min. Fixed and permeabilized cells were stained with rhodamine-phalloidin (left column) and with anti-cortactin (center column). Rhodamine images to detect F-actin (red) and Alexa 488 images for cortactin visualized by

cAMP-Epac-Rap1 signaling may contribute to the potentiation of endothelial barrier function and VE-cadherin-dependent cell adhesion.

DISCUSSION

cAMP is a well-known intracellular signaling molecule that is capable of restoring diminished endothelial barrier function. Previous reports suggested that cAMP-induced barrier enhancement occurs through PKA (27, 39). In this study, however, we demonstrated a novel PKA-independent signaling pathway, the cAMP-Epac-Rap1 signaling pathway, involved in cAMP-induced barrier function based on the following observations. PGI₂- and FSK-reduced endothelial permeability was insensitive to H89. A specific activator for Epac, 8-CPT-2'-O-Me-cAMP, reduced both basal and thrombin-increased permeability. Plasma leakage in response to VEGF was also inhibited by 8-CPT-2'-O-Me-cAMP in vivo. We found that the activation of Rap1 leads to decreased permeability. Not only all cAMP-elevating bio-ligands we tested but also FSK, db-cAMP, and IBMX activated Rap1. Consistently, cAMP-dependent Rap1 activation upon stimulation by these ligands involved Epac in the regulation of barrier function. A previous report showed that Rap1 is phosphorylated by PKA in neutrophils and platelets, although the function of phosphorylated Rap1 has not been elucidated (37). So far, Epac is known to regulate several biological functions including integrin-dependent cell adhesion, insulin secretion, and calcium release through ryanodine-sensitive Ca²⁺ channels (reviewed in reference 5). In addition to these Epac-mediated functions, we show, for the first time, that Epac-Rap1 signaling is important for regulation of endothelial barrier function.

AJ assembly contributes to the regulation of barrier function. Rap1 is involved in the formation and maintenance of AJ constituted by cadherin (23, 41). Recently, it has been reported that homophilic ligation of E-cadherin induced Rap1 activation, which may be responsible for maturation of AJ (20). Consistently, suppression of endogenous Rap1 inhibits formation of E-cadherin-dependent cell adhesion (36), suggesting the critical role of Rap1 in the establishment of cadherin-based cell-cell contacts. Here, we demonstrate that Rap1 also acts downstream of cAMP-Epac to potentiate VE-cadherin-depen-

Alexa 488-labeled secondary antibody (green) were obtained through a confocal microscope (BX50WI). Right panels show the merged images of rhodamine and Alexa 488 images. Bars, 20 μ m. (B) HUVECs transfected with an EGFP-expressing vector (left) and pCXN2-Rap1(GAPII-IRES-EGFP) (right) were serum starved in 0.5% BSA-containing medium 199 for 3 h and stimulated with vehicle (top panels) and 10 μ M FSK (bottom panels). Cells were fixed, permeabilized, and stained with Rhodamine-phalloidin. EGFP images (green) and rhodamine images showing F-actin (red) were obtained similar to those in panel A. Arrows and arrowhead indicate transfected and untransfected cells, respectively. Bars, 20 μ m. (C) Cell permeability of HUVECs pretreated with 2 μ M cytochalasin D (CytoD) for 30 min followed by 10 μ M FSK stimulation for 30 min was analyzed as described in the legend to Fig. 1A. -, absent; +, present. (D) The effect of pretreatment of 2 μ M cytochalasin D (CytoD) on adhesion of HUVECs stimulated with FSK was analyzed as described in the legend to Fig. 5E. A significant difference between two groups determined by Student's *t* test is indicated by double asterisks ($P < 0.01$).

dent cell adhesion, thereby improving barrier function. In addition to cAMP-elevating ligands, S1P, which enhances AJ formation and barrier function (18, 26), also activated Rap1 (our unpublished data). Thus, Rap1 may play a crucial role in barrier function induced by various types of barrier-improving factors.

Our data and previous studies show that cAMP protects thrombin-induced endothelial barrier dysfunction. cAMP does not limit the effect of thrombin on the initial loss of endothelial barrier (32). Instead, cAMP enhances the restoration of barrier function disrupted by thrombin. Recently, it was also reported that Cdc42 regulates the restoration of endothelial barrier function disrupted by thrombin (24). Thus, cAMP-Epac-Rap1 signaling may facilitate the formation of VE-cadherin-based cell-cell contacts, cooperatively or in parallel with Cdc42.

Rap1 enhances integrin-dependent cell adhesion in a variety of hematopoietic cells by modulating the affinity and avidity of integrin (6, 22). Cell adhesion to VEC-Fc-coated dishes was augmented by Rap1 activation, suggesting that the homophilic binding of VE-cadherin is also likely ascribed to the affinity and avidity of VE-cadherin modulated by Rap1-triggered inside out signaling. Hogan et al. reported that Rap1 activity is required for the targeting of E-cadherin molecules into nascent cell-cell contact sites, which in turn leads to the maturation of E-cadherin-based cell-cell contacts (20). Thus, cAMP-Epac-Rap1 signaling may also regulate the recruitment of VE-cadherin into maturing cell-cell contacts. Since downstream signaling of Rap1 that increases homophilic binding of VE-cadherin has not yet been characterized, the effector of cAMP-Epac-Rap1 signaling will need to be identified.

The actin cytoskeleton is a critical determinant of vascular integrity (10). PGI₂, FSK, and 8-CPT-2'-O-Me-cAMP induced cortical actin rearrangement in a Rap1-dependent manner. FSK-induced VE-cadherin-dependent cell adhesion was inhibited by cytochalasin D. Thus, Rap1 may promote VE-cadherin-dependent cell adhesion by inducing cortical actin rearrangement. AF-6 may act downstream of Rap1 to regulate the actin cytoskeleton, since it binds to GTP-bound Rap1 and the actin cytoskeleton regulator, profilin, and is localized at AJ (2). Consistently, Canoe, the drosophila homolog of AF-6, and Rap1 function in the same molecular pathway during embryonic dorsal closure, which requires cell-cell contacts (3). S1P promotes endothelial barrier function by inducing Rac-dependent cortical actin rearrangement. S1P also induces Rap1 activation (our unpublished data). A previous report indicates that Rac can function downstream of Rap1 in the processing of the amyloid precursor protein (28). Taken together, Rac may act downstream of Rap1 to induce cortical actin rearrangement.

In conclusion, we have demonstrated that the cAMP-Epac-Rap1 signaling pathway promotes VE-cadherin-mediated cell adhesion and consequently improves endothelial barrier function.

ACKNOWLEDGMENTS

We thank J. L. Bos and W. A. Muller for plasmids, M. Matsuda and S. Hattori for adenovirus, J. T. Pearson for critical reading, and M. Sone, K. Yamamoto, and N. Irisawa for technical assistance.

This work was supported by grants from the Ministry of Health, Labor, and Welfare of Japan, from the Promotion of Fundamental Studies in Health Science of the Organization for Pharmaceutical Safety and Research of Japan, from the Ministry of Education, Science, Sports, and Culture of Japan, from the Uehara Memorial Foundation, and from Senri Life Science Foundation.

REFERENCES

- Andriopoulou, P., P. Navarro, A. Zanetti, M. G. Lampugnani, and E. Dejana. 1999. Histamine induces tyrosine phosphorylation of endothelial cell-to-cell adherens junctions. *Arterioscler. Thromb. Vasc. Biol.* **19**:2286–2297.
- Boettner, B., E. E. Govek, J. Cross, and L. Van Aelst. 2000. The junctional multidomain protein AF-6 is a binding partner of the Rap1A GTPase and associates with the actin cytoskeletal regulator profilin. *Proc. Natl. Acad. Sci. USA* **97**:9064–9069.
- Boettner, B., P. Harjes, S. Ishimaru, M. Heke, H. Q. Fan, Y. Qin, L. Van Aelst, and U. Gaul. 2003. The AF-6 homolog canoe acts as a Rap1 effector during dorsal closure of the *Drosophila* embryo. *Genetics* **165**:159–169.
- Bogatcheva, N. V., J. G. Garcia, and A. D. Verin. 2002. Molecular mechanisms of thrombin-induced endothelial cell permeability. *Biochemistry (Moscow)* **67**:75–84.
- Bos, J. L. 2003. Epac: a new cAMP target and new avenues in cAMP research. *Nat. Rev. Mol. Cell Biol.* **4**:733–738.
- Bos, J. L., J. de Rooij, and K. A. Reedquist. 2001. Rap1 signalling: adhering to new models. *Nat. Rev. Mol. Cell Biol.* **2**:369–377.
- Chijiwa, T., A. Mishima, M. Hagiwara, M. Sano, K. Hayashi, T. Inoue, K. Naito, T. Toshioka, and H. Hidaka. 1990. Inhibition of forskolin-induced neurite outgrowth and protein phosphorylation by a newly synthesized selective inhibitor of cyclic AMP-dependent protein kinase, N-[2-(p-bromocinamylamino)ethyl]-5-isoquinolinesulfonamide (H-89), of PC12D pheochromocytoma cells. *J. Biol. Chem.* **265**:5267–5272.
- Daly, R. J. 2004. Cortactin signalling and dynamic actin networks. *Biochem. J.* **382**:13–25. [Online.] doi:10.1042/BJ20040737.
- Dejana, E. 2004. Endothelial cell-cell junctions: happy together. *Nat. Rev. Mol. Cell Biol.* **5**:261–270.
- Dudek, S. M., and J. G. Garcia. 2001. Cytoskeletal regulation of pulmonary vascular permeability. *J. Appl. Physiol.* **91**:1487–1500.
- Dudek, S. M., J. R. Jacobson, E. T. Chiang, K. G. Birukov, P. Wang, X. Zhan, and J. G. Garcia. 2004. Pulmonary endothelial cell barrier enhancement by sphingosine 1-phosphate: roles for cortactin and myosin light chain kinase. *J. Biol. Chem.* **279**:24692–24700.
- Endo, A., K. Nagashima, H. Kurose, S. Mochizuki, M. Matsuda, and N. Mochizuki. 2002. Sphingosine 1-phosphate induces membrane ruffling and increases motility of human umbilical vein endothelial cells via vascular endothelial growth factor receptor and CrkII. *J. Biol. Chem.* **277**:23747–23754.
- Enserink, J. M., A. E. Christensen, J. de Rooij, M. van Triest, F. Schwede, H. G. Genieser, S. O. Doskeland, J. L. Blank, and J. L. Bos. 2002. A novel Epac-specific cAMP analogue demonstrates independent regulation of Rap1 and ERK. *Nat. Cell Biol.* **4**:901–906.
- Esser, S., M. G. Lampugnani, M. Corada, E. Dejana, and W. Risau. 1998. Vascular endothelial growth factor induces VE-cadherin tyrosine phosphorylation in endothelial cells. *J. Cell Sci.* **111**(Pt 13):1853–1865.
- Farmer, P. J., S. G. Bernier, A. Lepage, G. Guillemette, D. Regoli, and P. Sirois. 2001. Permeability of endothelial monolayers to albumin is increased by bradykinin and inhibited by prostaglandins. *Am. J. Physiol. Lung Cell. Mol. Physiol.* **280**:L732–L738.
- Fukuhara, S., M. J. Marinissen, M. Chiariello, and J. S. Gutkind. 2000. Signaling from G protein-coupled receptors to ERK5/Big MAPK 1 involves G α q and G α 12/13 families of heterotrimeric G proteins. Evidence for the existence of a novel Ras AND Rho-independent pathway. *J. Biol. Chem.* **275**:21730–21736.
- Gamble, J. R., J. Drew, L. Trezise, A. Underwood, M. Parsons, L. Kasminkas, J. Rudge, G. Yancopoulos, and M. A. Vadas. 2000. Angiopoietin-1 is an antipermeability and anti-inflammatory agent in vitro and targets cell junctions. *Circ. Res.* **87**:603–607.
- Garcia, J. G., F. Liu, A. D. Verin, A. Birukova, M. A. Dechert, W. T. Gerthoffer, J. R. Bamberg, and D. English. 2001. Sphingosine 1-phosphate promotes endothelial cell barrier integrity by Edg-dependent cytoskeletal rearrangement. *J. Clin. Investig.* **108**:689–701.
- Hippenstiel, S., M. Witzernath, B. Schmeck, A. Hocke, M. Krisp, M. Krull, J. Seybold, W. Seeger, W. Rascher, H. Schutte, and N. Suttrop. 2002. Adrenomedullin reduces endothelial hyperpermeability. *Circ. Res.* **91**:618–625.
- Hogan, C., N. Serpente, P. Cogram, C. R. Hosking, C. U. Bialucha, S. M. Feller, V. M. M. Braga, W. Birchmeier, and Y. Fujita. 2004. Rap1 regulates the formation of E-cadherin-based cell-cell contacts. *Mol. Cell. Biol.* **24**:6690–6700.
- Kawasaki, H., G. M. Springett, N. Mochizuki, S. Toki, M. Nakaya, M. Matsuda, D. E. Housman, and A. M. Graybiel. 1998. A family of cAMP-binding proteins that directly activate Rap1. *Science* **282**:2275–2279.
- Kimbara, K., L. E. Goldfinger, M. Hansen, F. L. Chou, and M. H. Ginsberg.

2003. Ras GTPases: integrins' friends or foes? *Nat. Rev. Mol. Cell Biol.* **4**:767–776.
23. Knox, A. L., and N. H. Brown. 2002. Rap1 GTPase regulation of adherens junction positioning and cell adhesion. *Science* **295**:1285–1288.
 24. Kouklis, P., M. Konstantoulaki, S. Vogel, M. Broman, and A. B. Malik. 2004. Cdc42 regulates the restoration of endothelial barrier function. *Circ. Res.* **94**:159–166.
 25. Langeler, E. G., and V. W. van Hinsbergh. 1991. Norepinephrine and iloprost improve barrier function of human endothelial cell monolayers: role of cAMP. *Am. J. Physiol.* **260**:C1052–C1059.
 26. Lee, M. J., S. Thangada, K. P. Claffey, N. Ancellin, C. H. Liu, M. Kluk, M. Volpi, R. I. Sha'afi, and T. Hla. 1999. Vascular endothelial cell adherens junction assembly and morphogenesis induced by sphingosine-1-phosphate. *Cell* **99**:301–312.
 27. Lum, H., H. A. Jaffe, I. T. Schulz, A. Masood, A. RayChaudhury, and R. D. Green. 1999. Expression of PKA inhibitor (PKI) gene abolishes cAMP-mediated protection to endothelial barrier dysfunction. *Am. J. Physiol.* **277**:C580–C588.
 28. Maillet, M., S. J. Robert, M. Cacquevel, M. Gastineau, D. Vivien, J. Bertoglio, J. L. Zugaza, R. Fischmeister, and F. Lezoualc'h. 2003. Crosstalk between Rap1 and Rac regulates secretion of sAPPalpha. *Nat. Cell Biol.* **5**:633–639.
 29. Miles, A. A., and E. M. Miles. 1952. Vascular reactions to histamine, histamine-liberator and leukotaxine in the skin of guinea-pigs. *J. Physiol.* **118**:228–257.
 30. Mochizuki, N., Y. Ohba, E. Kiyokawa, T. Kurata, T. Murakami, T. Ozaki, A. Kitabatake, K. Nagashima, and M. Matsuda. 1999. Activation of the ERK/MAPK pathway by an isoform of rap1GAP associated with G alpha(i). *Nature* **400**:891–894.
 31. Mori, Y., T. Nishikimi, N. Kobayashi, H. Ono, K. Kangawa, and H. Matsuo. 2002. Long-term adrenomedullin infusion improves survival in malignant hypertensive rats. *Hypertension* **40**:107–113.
 32. Moy, A. B., J. E. Bodmer, K. Blackwell, S. Shasby, and D. M. Shasby. 1998. cAMP protects endothelial barrier function independent of inhibiting MLC20-dependent tension development. *Am. J. Physiol.* **274**:L1024–L1029.
 33. Navarro, P., L. Ruco, and E. Dejana. 1998. Differential localization of VE- and N-cadherins in human endothelial cells: VE-cadherin competes with N-cadherin for junctional localization. *J. Cell Biol.* **140**:1475–1484.
 34. Ohba, Y., K. Ikuta, A. Ogura, J. Matsuda, N. Mochizuki, K. Nagashima, K. Kurokawa, B. J. Mayer, K. Maki, J. Miyazaki, and M. Matsuda. 2001. Requirement for C3G-dependent Rap1 activation for cell adhesion and embryogenesis. *EMBO J.* **20**:3333–3341.
 35. Parandoosh, Z., C. A. Bogowitz, and M. P. Nova. 1998. A fluorometric assay for the measurement of endothelial cell density in vitro. *In Vitro Cell. Dev. Biol. Anim.* **34**:772–776.
 36. Price, L. S., A. Hajdo-Milasinovic, J. Zhao, F. J. Zwartkruis, J. G. Collard, and J. L. Bos. 2004. Rap1 regulates E-cadherin-mediated cell-cell adhesion. *J. Biol. Chem.* **279**:35127–35132.
 37. Quilliam, L. A., H. Mueller, B. P. Bohl, V. Prossnitz, L. A. Sklar, C. J. Der, and G. M. Bokoch. 1991. Rap1A is a substrate for cyclic AMP-dependent protein kinase in human neutrophils. *J. Immunol.* **147**:1628–1635.
 38. Shaywitz, A. J., and M. E. Greenberg. 1999. CREB: a stimulus-induced transcription factor activated by a diverse array of extracellular signals. *Annu. Rev. Biochem.* **68**:821–861.
 39. Stelzner, T. J., J. V. Weil, and R. F. O'Brien. 1989. Role of cyclic adenosine monophosphate in the induction of endothelial barrier properties. *J. Cell. Physiol.* **139**:157–166.
 40. Ukropec, J. A., M. K. Hollinger, S. M. Salva, and M. J. Woolkalis. 2000. SHP2 association with VE-cadherin complexes in human endothelial cells is regulated by thrombin. *J. Biol. Chem.* **275**:5983–5986.
 41. Yajnik, V., C. Paulding, R. Sordella, A. I. McClatchey, M. Saito, D. C. Wahrer, P. Reynolds, D. W. Bell, R. Lake, S. van den Heuvel, J. Settleman, and D. A. Haber. 2003. DOCK4, a GTPase activator, is disrupted during tumorigenesis. *Cell* **112**:673–684.
 42. Yano, H., Y. Mazaki, K. Kurokawa, S. K. Hanks, M. Matsuda, and H. Sabe. 2004. Roles played by a subset of integrin signaling molecules in cadherin-based cell-cell adhesion. *J. Cell Biol.* **166**:283–295.
 43. Yuan, S. Y. 2002. Protein kinase signaling in the modulation of microvascular permeability. *Vascul. Pharmacol.* **39**:213–223.



Functional heterogeneity of side population cells in skeletal muscle

Akiyoshi Uezumi, Koichi Ojima, So-ichiro Fukada, Madoka Ikemoto, Satoru Masuda,
Yuko Miyagoe-Suzuki, Shin'ichi Takeda *

*Department of Molecular Therapy, National Institute of Neuroscience, National Center of Neurology and Psychiatry,
4-1-1 Ogawa-higashi, Kodaira, Tokyo 187-8502, Japan*

Received 18 December 2005
Available online 23 January 2006

Abstract

Skeletal muscle regeneration has been exclusively attributed to myogenic precursors, satellite cells. A stem cell-rich fraction referred to as side population (SP) cells also resides in skeletal muscle, but its roles in muscle regeneration remain unclear. We found that muscle SP cells could be subdivided into three sub-fractions using CD31 and CD45 markers. The majority of SP cells in normal non-regenerating muscle expressed CD31 and had endothelial characteristics. However, CD31⁺CD45⁺ SP cells, which are a minor subpopulation in normal muscle, actively proliferated upon muscle injury and expressed not only several regulatory genes for muscle regeneration but also some mesenchymal lineage markers. CD31⁺CD45⁺ SP cells showed the greatest myogenic potential among three SP sub-fractions, but indeed revealed mesenchymal potentials *in vitro*. These SP cells preferentially differentiated into myofibers after intramuscular transplantation *in vivo*. Our results revealed the heterogeneity of muscle SP cells and suggest that CD31⁺CD45⁺ SP cells participate in muscle regeneration.

© 2006 Elsevier Inc. All rights reserved.

Keywords: Side population cells; Muscle regeneration; Mesenchymal differentiation; Transplantation

Adult skeletal muscles have a remarkable ability to regenerate following muscle damage. This regeneration has been attributed to satellite cells that reside between the sarcolemma and the basal lamina. Satellite cells are quiescent mononucleated cells in normal conditions, however, in response to muscle damage, they become activated, proliferate, and then exit the cell cycle either to renew the quiescent satellite cell pool or to differentiate into mature myofibers. Thus, they have been considered to be the myogenic precursor cells that give rise to myoblasts and the sole source of adult myogenic cells [1].

In 1998, Ferrari et al. [2] have demonstrated for the first time that bone marrow (BM)-derived cells contribute to the skeletal muscle after BM transplantation. Side population (SP) cells were first identified in bone marrow based on the ability to exclude Hoechst 33342 dye as an enriched

fraction of hematopoietic stem cells (HSCs) [3], later, it has been reported that they also participate in muscle regeneration [4]. Studies using whole BM cells showed that BM-derived mononucleated cells display several characteristics of satellite cells, suggesting that donor-derived BM cells contribute to muscle fibers in a stepwise biological progression [5,6]. However, using single HSC transplantation experiment, Camargo et al. [7] suggested that cells committed to the myeloid lineage contribute to muscle through fusion event. Therefore, multiple mechanisms underlay contribution of BM-derived cells to skeletal muscle regeneration.

SP cells have been also identified in skeletal muscle [4]. Muscle SP cells cannot only reconstitute the hematopoietic system of lethally irradiated mice [4,8], but also differentiate into skeletal muscle cells [4,9]. Furthermore, they have been reported to participate in vascular regeneration [10]. Several lines of evidence suggest that muscle SP cells are a cell population distinct from satellite cells [9,11–13]. While muscle SP cells possess these attractive

* Corresponding author. Fax: +81 42 346 1750.
E-mail address: takeda@nnp.go.jp (S. Takeda).

features, they have been reported to be heterogeneous population. In fact, muscle SP cells contain both CD45⁺ and CD45⁻ cells, and hematopoietic potential has been exclusively found in CD45⁺ fraction [8,9]. As regards the myogenic potential, both CD45⁺ and CD45⁻ fractions have been shown to differentiate into skeletal muscle cells [9,14], but there is no comparative study dealing with subpopulation of muscle SP cells during muscle regeneration.

In the present study, we have further divided muscle SP cells into three sub-fractions using CD31 and CD45, examined the properties of each sub-fraction, and identified a novel subpopulation (CD31⁺ CD45⁻ SP cells) that showed the greatest myogenic potential both in vitro and in vivo. These results provide a new insight for stem cell-based therapy of muscular dystrophy.

Materials and methods

Animals. All procedures using experimental animals were approved by the Experimental Animal Care and Use Committee at the National Institute of Neuroscience. Eight- to ten-week-old C57BL/6 mice were purchased from Nihon CLEA (Japan). GFP Tg mice were provided by Dr. M. Okabe (Osaka University) and used in cell transplantation experiments. NOD/scid mice provided by the Institute for Experimental Animals, Japan, were used as recipients.

To induce muscle regeneration, 100 μ l of CTX (10 μ M in saline, Wako Chemicals) was injected into the tibialis anterior (TA) muscle with a 29-gauge needle. In FACS analysis experiments, CTX was injected into TA (50 μ l), gastrocnemius (50 μ l), and quadriceps femoris muscles (25 μ l).

BM transplantation was performed as previously described [14]. Mice were subjected to analysis 12 weeks after transplantation.

Antibodies. Mouse Berp-1 cDNA was provided by Dr. A.H. Schinkel [15]. A DNA fragment corresponding to cytoplasmic domain of Berp1, amino acids 300–337, was fused to GST in a pGEX-4T-2 vector (Amersham Biosciences), and the fusion protein was used to immunize rabbits. The serum obtained was affinity-purified. Other antibodies used in these studies are listed in Table S1.

Cell preparation and FACS analysis. Muscle-derived mononucleated cells were prepared from C57BL/6 mice, GFP Tg mice, or GFP-BM transplanted mice as previously described [14]. Hoechst staining was performed as described by Goodell et al. (http://www.bem.tmc.edu/genetherapy/goodell/new_site/protocols.html). Cells were re-suspended at 10⁶ cells per ml in DMEM (Invitrogen) containing 2% FBS (Trace Biosciences), 10 mM HEPES, and 5 μ g/ml Hoechst 33342 (Sigma), and incubated for 90 min at 37 °C in the presence or the absence of 50 μ M verapamil (Sigma). During incubation, cells were mixed 3–4 times. For analysis of Ac-LDL uptake, 10 μ g/ml DiI-labeled Ac-LDL (Biomedical Technologies) was added. After antibody staining, cells were re-suspended in PBS containing 2.5% FBS and 2 μ g/ml propidium iodide (PI) (BD Pharmingen). Cell sorting was performed on a FACS VantageSE flow cytometer (BD Biosciences). Debris and dead cells were excluded by forward scatter, side scatter, and PI gating. Cell viability after staining and sorting was comparable to that previously reported [14].

RNA extraction and RT-PCR. Total RNA was extracted from 1 \times 10⁴ FACS sorted cells by using a RNeasy Micro Kit (Qiagen) and then reverse transcribed into cDNA by using TaqMan Reverse Transcription Reagents (Roche). The PCRs were performed with 1 μ l cDNA product under the following cycling conditions: 94 °C for 3 min followed by 40 cycles of amplification (94 °C for 15 s, 60 °C for 30 s, and 72 °C for 30 s) with a final incubation at 72 °C for 5 min. Specific primer sequences used for PCR are available on request.

Cell culture. SP cells were cultured alone with growth medium (GM): DMEM containing 20% FBS and 2.5 ng/ml bFGF (Invitrogen) in chamber slides (Nalge Nunc) coated with Matrigel (BD Biosciences) for 3–5 days. For osteogenic differentiation, the medium was changed to a differentiation medium (DM), 5% horse serum in DMEM supplemented with or without 500 ng/ml recombinant human BMP2 (R&D Systems), and cultured for 4–6 days. For adipogenic differentiation, cells were exposed to 3 cycles of 3 days of adipogenic induction medium (Cambrex Bioscience) followed by 1 day of adipogenic maintenance medium (Cambrex Bioscience) and then cells were maintained for five more days in the adipogenic maintenance medium. Alkaline phosphatase (AP) was stained using Sigma kit #85 according to the manufacturer's instructions. To stain lipids, cells were fixed in 10% formalin, rinsed in water and then 60% isopropanol, stained with Oil red O in 60% isopropanol, and rinsed in water. For myogenic differentiation, muSP-31, muSP-45, or muSP-DN purified from GFP Tg mice were co-cultured with myoblasts prepared from C57BL/6 mice as previously described [16,17] in GM. DM was supplied 3–5 days after starting co-culture.

Osteogenic activity and myotube-forming activity were determined by the following formulas: osteogenic activity = [(the number of AP⁺ cells in seven randomly selected fields (corresponding to one-tenth of the whole area of the well))/(the number of seeded cells)] and myotube-forming activity = (the number of GFP⁺ myotubes in seven randomly selected fields)/(the number of seeded cells). In order to measure the extent of adipogenic differentiation, stained oil droplets were extracted for 5 min with 100 μ l of 4% Nonidet P-40 in isopropanol, and the absorbance of the dye-triglyceride complex was measured at 520 nm [18]; then, adipogenic activity was determined by the following formula: (the absorbance at 520 nm)/(the number of seeded cells).

Intramuscular transplantation experiments. muSP-DN or muSP-31 cells were purified from GFP Tg mice and were injected directly into the TA muscles of NOD/scid mice. One day before transplantation, host TA muscles were treated with CTX. The number of transplanted cells is indicated in Table 1. Three weeks after transplantation, TA muscles were excised and fixed in 4% PFA for 30 min, immersed sequentially in 10% sucrose/PBS and 20% sucrose/PBS, and frozen in isopentane cooled with liquid nitrogen.

Immunohistochemistry. FACS sorted cells were collected by Cytospin3 (ThermoShandon). Cells were fixed with 4% PFA for 5 min. Frozen muscle tissues were sectioned using a cryostat. Specimens were blocked with 5% goat serum (Cedarlane) in PBS for 15 min and incubated with primary antibodies at 4 °C overnight, followed by secondary staining. Stained cells were mounted in Vectashield with DAPI (Vector) and photographed using a fluorescence microscope IX70 (OLYMPUS) equipped with a QuantixTM air-cooled CCD camera (Photometrics) and IP Lab software (Scanalytics Inc.). Stained muscle sections were counterstained with TOTO-3 (1:5000; Molecular Probes), then mounted in Vectashield (Vector), and observed under the confocal laser scanning microscope system TCS SP (Leica).

Statistics. Values were expressed as means \pm SD or \pm SEM. Statistical significance was assessed by Student's *t* test. In comparison of more than two groups, one-way analysis of variance (ANOVA) followed by the Fisher's PLSD was used. A probability of less than 5% (*P* < 0.05) or 1% (*P* < 0.01) was considered statistically significant.

Table 1
Appearance of GFP⁺ myofibers after intramuscular transplantation

Cell type	Experiment No.	Number of injected cells/TA muscle	Number of GFP ⁺ myofibers/TA muscle
muSP-DN cells	Ex. 1	1.7 \times 10 ³	14
	Ex. 2	2.5 \times 10 ³	9
	Ex. 3	2.5 \times 10 ³	0
muSP-31 cells	Ex. 1	1.6 \times 10 ⁴	3
	Ex. 2	1.6 \times 10 ⁴	0
	Ex. 3	1.6 \times 10 ⁴	0

Results

Most muscle SP cells are found in a subset of capillary or vein endothelial cells in non-regenerating skeletal muscle

We identified verapamil-sensitive SP cells in skeletal muscle after Hoechst staining (Fig. 1A) and analyzed the expression of several markers on them. The majority of muscle SP cells were CD31⁺, usually recognized as a marker of endothelial cells (Figs. 1B–E), and negative for a pan-hematopoietic marker, CD45 (Fig. 1B). More than half of muscle SP cells were CD34⁺, and Sca-1⁺ cells comprised 90% of muscle SP cells (Figs. 1C and D). Compared to FACS profiles of whole-muscle-derived cells, SP cells were enriched in Sca-1⁺ cells (Fig. S1). More than 85% of muscle SP cells were CD31⁺ and took up acetylated low-density lipoprotein (Ac-LDL), a functional marker for endothelial cells and macrophages (Fig. 1E). These results indicate that most muscle SP cells have endothelial characteristics. Only cells in the main population (MP) were found to be Pax7⁺, indicating that SP cells do not include muscle satellite cells (data not shown).

To examine the localization of muscle SP cells, we generated a rabbit polyclonal anti-mouse Berp1 antibody, because it has been reported that Berp1 is the major determinant of the SP phenotype [19]. Our antibody clearly recognized Berp1 expression in liver, small intestine, and kidney, as previously reported (Fig. S2) [20,21]. We confirmed that Berp1 antibody recognizes more than 80% of SP cells and less than 3% of MP cells collected by cytopsin (Figs. 1F and G). In skeletal muscle, Berp1⁺ cells were found outside the muscle basal lamina (Fig. 1H), which clearly distinguished Berp1⁺ cells from satellite cells. Next, Berp1 expression in the vascular system was investigated. CD31 staining identified all endothelia from larger vessels to capillaries in muscle sections. Intriguingly, Berp1 was expressed by CD31-expressing endothelial cells, and its expression was preferentially observed on a subpopulation of capillary endothelium (Figs. 1I–K) and venous endothelium surrounded by thin vessel walls, as revealed by α -smooth muscle actin (α SMA) expression (Figs. 1L–N). These results, together with the results of FACS analysis, strongly suggest that the majority of muscle SP cells are a subset of endothelial cells present in capillaries or veins in non-regenerating skeletal muscle.

Behavior of muscle SP cells during muscle regeneration

We next examined the kinetics of SP cells during muscle regeneration induced by injection of cardiotoxin (CTX). After CTX injection, the total number of mononuclear cells per muscle weight gradually increased, with a peak at day 3. The number of SP cells also increased and reached its peak at day 3 (Fig. 2A). Muscle SP cells could be divided into three subpopulations based on CD31 and CD45 expression: CD31⁺CD45[−] SP cells (designated muSP-31 cells), CD31⁺CD45⁺ SP cells (muSP-45 cells), and

CD31[−]CD45[−] SP cells (muSP-DN cells). muSP-31 cells and muSP-DN cells distributed throughout the SP tail, but muSP-45 cells were located close to the shoulder (data not shown). The majority of muscle SP cells in untreated muscle were muSP-31 cells (Fig. 1B). During regeneration, however, muSP-45 cells and muSP-DN cells increased in both their ratios and their numbers (Figs. 2B and C). Although CD45⁺ cells were abundant in whole muscle-derived cells during regeneration and most of them were F4/80 antigen-positive mature macrophages, SP cells did not contain any mature inflammatory cells, as previously reported (data not shown) [14].

To clarify the origin of each subpopulation of SP cells, BM transplantation experiments were performed. We confirmed that muSP-45 cells were mobilized from bone marrow as previously reported (Figs. 3A and B) [14]. In contrast, both CD45[−] SP fractions are residents of skeletal muscle (Figs. 3A and B), consistent with the results reported by Rivier et al. [22].

Next, to determine whether each subpopulation of SP cells proliferates in damaged muscle, cells were stained with Ki67 antibody. Most muSP-45 cells (Figs. 3C and D) and muSP-31 cells (Figs. 3G and H) prepared from regenerating muscle were negative for Ki67, suggesting that the proliferation activities of these two fractions were low. On the other hand, about 60% of muSP-DN cells were positive for Ki67 (Figs. 3E and F), indicating that muSP-DN cells actively proliferated during muscle regeneration.

We next examined Berp1 expression on three sub-fractionated SP cells and found that only muSP-31 cells were Berp1-positive (Fig. 3K). These results suggest that some ABC transporters other than Berp1 are responsible for the phenotype of CD31⁺ SP cells.

Gene expression of muscle SP cells during muscle regeneration

Our analysis revealed that each subpopulation of SP cells showed distinct kinetics during muscle regeneration. To better understand the traits of muscle SP cells, we analyzed gene expression during muscle regeneration. Three subpopulations of SP cells (in following experiments, muSP-45 cells from untreated muscle were omitted because of their low yield) or MP cells were collected from each time point during muscle regeneration, and RT-PCR was performed. We chose several myogenic (*Pax3*, *Pax7*, and *myf5*), endothelial (*Tie2*, *Flk1*, and *eWf*), and mesodermal-mesenchymal-associated (α SMA, *PPAR γ* , *Runx2*, *PDGFR α* , and *PDGFR β*) genes to clarify lineage characteristics of the target cells. We also examined expression of genes of developmental regulators (*msx1*, *Frizzled4* (*Fzd4*), *Patched1* (*Ptc1*), and *BMPRIA*), angiogenic factors (*angiopoietin-1* (*ang1*) and *VEGF*), and TGF- β superfamily antagonists (*follicle-stimulating hormone* (*FSH*) and *DAN*), muSP-DN cells from untreated muscles expressed only *PDGFR β* , *Ptc1*, *ang1*, *follicle-stimulating hormone*, and *DAN* (Fig. 4, cont. lane 1). Neither myogenic nor other lineage-specific markers could be detected in

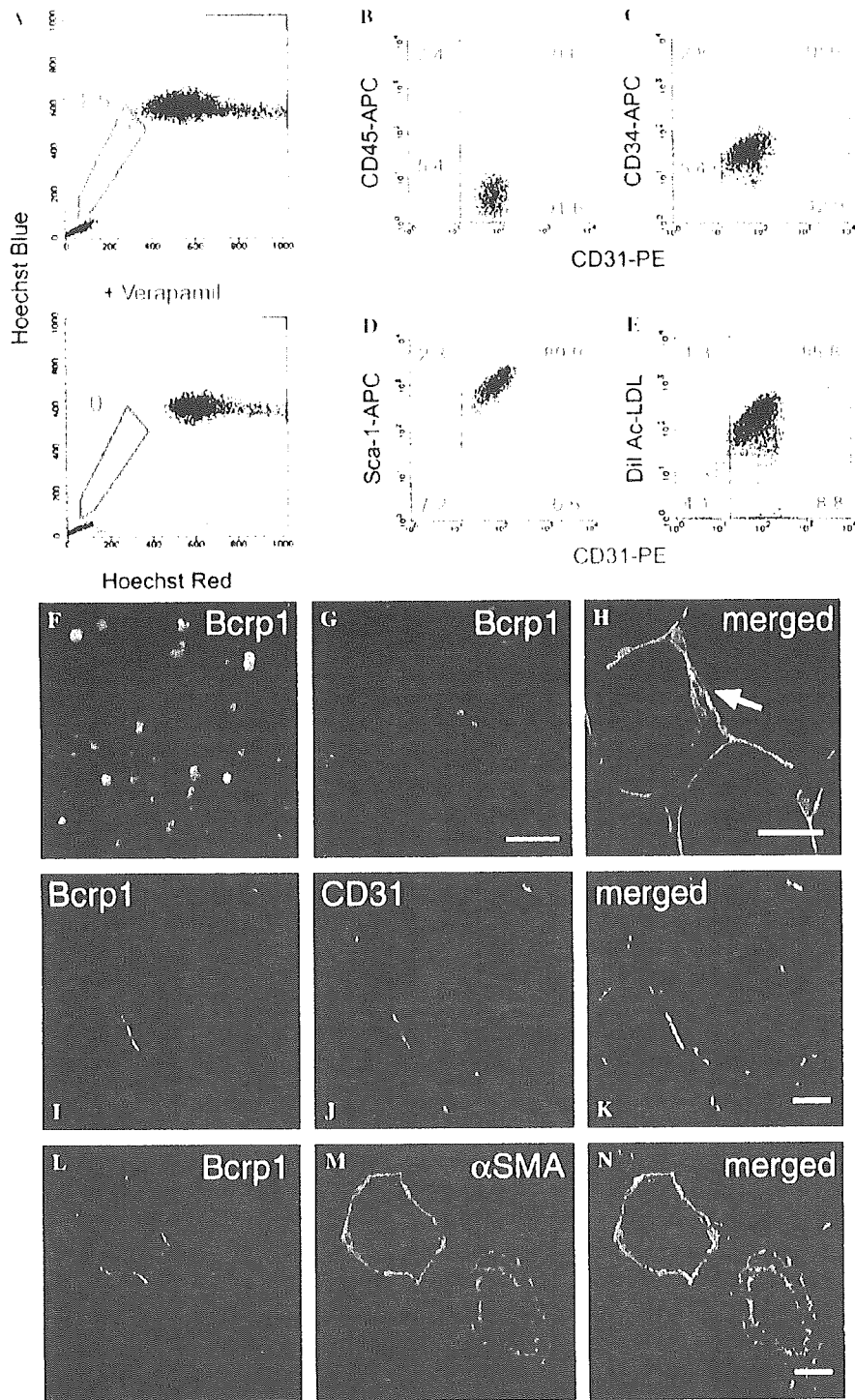


Fig. 1. Characterization of skeletal muscle SP cells. (A) Flow cytometric analysis of muscle-derived mononucleated cells after Hoechst 33342 staining with (lower panel) or without Verapamil (upper panel). The numbers indicate the percentage of SP cells (blue pentagons) in all mononucleated cells. (B–E) The expression of CD45 (B), CD34 (C), Sca-1 (D), and DiI-Ac-LDL uptake (E), and CD31 (B–E) on muscle SP cells. The percentage of cells in each quadrant is shown in the panel. (F,G) Immunofluorescent staining for Bcrp1 (green) and DAPI counterstaining (blue) of freshly sorted SP (F) and MP (G) cells. Immunofluorescent staining for Bcrp1 (green) and laminin $\gamma 2$ chain (red) (H), Bcrp1 (green) and CD31 (red) (I–K), and Bcrp1 (green) and α -smooth muscle actin (red) (L–N). TOYO-3 nuclear staining is shown in merged images (blue in H, K, and N). Bcrp1-positive cells are located outside the basal lamina (arrow), and they are partially overlapped with endothelial cells of capillary (I–K) and vein (L–N). Bars: 50 μ m in (F,G), 20 μ m in (H–N).

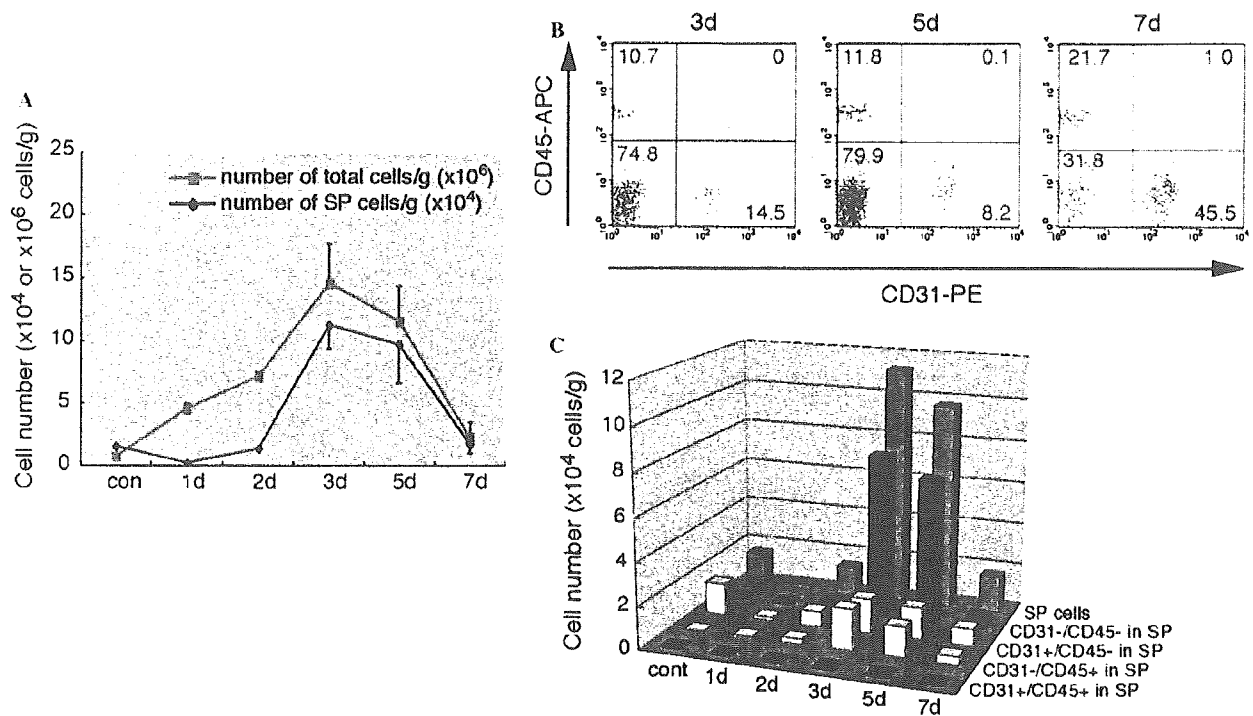


Fig. 2. Behavior of subpopulations of SP cells during muscle regeneration. (A) At 1 day (1d), 2 days (2d), 3 days (3d), 5 days (5d), and 7 days (7d) after CTX injection, the number of total cells (pink line) and SP cells (blue line) per gram of muscle weight was quantified. (B) At 3 days (3d), 5 days (5d), and 7 days (7d) after CTX injection, muscle SP cells prepared from regenerating muscle were analyzed for CD31 and CD45 expression. (C) Cell numbers in subpopulations of SP cells. muSP-45 cells (light blue bar) and muSP-DN cells (dark red bar) were significantly increased in number during muscle regeneration. Values (A,C) are the average of three independent experiments. Error bars represent SD.

this population indicating that muSP-DN cells do not contain cells committed to the lineages tested. At day 3 after CTX injection, muSP-DN cells began to express developmental regulator genes (Fig. 4, 3d, lane 1), and then at day 5, they also began to express several other lineage-specific genes (*Tie2*, α *SMA*, *PPAR γ* , and *Runx2*). Angiogenic factors and TGF- β superfamily antagonists were also strongly expressed at this time point (Fig. 4, 5d, lane 1). In contrast, muSP-31 cells continuously expressed all three endothelial genes analyzed throughout the regeneration process (Fig. 4, lane 2). Expression of mature endothelial marker, such as *vWF*, suggests that muSP-31 cells represent committed endothelial cells. muSP-45 cells expressed only low levels of α *SMA*, *PDGFR β* , and *follistatin* at day 5 after CTX injection (Fig. 4, lane 3). Myogenic markers, *Pax7* and *myf5*, were detected only in the MP fraction (Fig. 4, MP) indicating that myogenic cells are completely sorted into the MP fraction even during the process of muscle regeneration.

Differentiation potential of muscle SP cells for mesenchymal lineages

muSP-DN cells showed a unique gene expression pattern during muscle regeneration process: they began to express several mesenchymal genes at a late phase of muscle regeneration. Therefore, we examined the mesenchymal

potentials of muscle SP subpopulations. muSP-DN cells from untreated muscle readily gave rise to alkaline phosphatase (AP)-positive cells when cultured in the presence of bone morphogenetic protein 2 (BMP2) (Figs. 5A and C). With adipogenic induction, they also differentiated into adipocytes containing numerous lipid droplets in the cytoplasm (Figs. 5A and D). Reflecting the results of gene expression analysis, muSP-DN cells from regenerating muscle more efficiently differentiated into osteogenic cells and adipocytes than those from untreated muscle did (Figs. 5B–D). Unexpectedly, muSP-DN cells from regenerating muscle also differentiated into adipocytes without adipogenic induction (Figs. 5B and D), suggesting that they are susceptible to adipogenesis under our culture condition. In contrast, muSP-31 cells did not possess these differentiation potentials (Figs. 5A–D). Nor did muSP-45 cells, which were dramatically mobilized from BM into regenerating muscle (Figs. 5B–D). The attribute of differentiation potential is therefore a feature of muSP-DN.

Myogenic potential of muscle SP cells in vitro

We next evaluated the myogenic potential of muscle SP cells in vitro. When SP cells were cultured alone, they never differentiated into skeletal muscle cells (data not shown). Each subpopulation of SP cells was prepared from GFP Tg mice and co-cultured with wild type (WT) primary

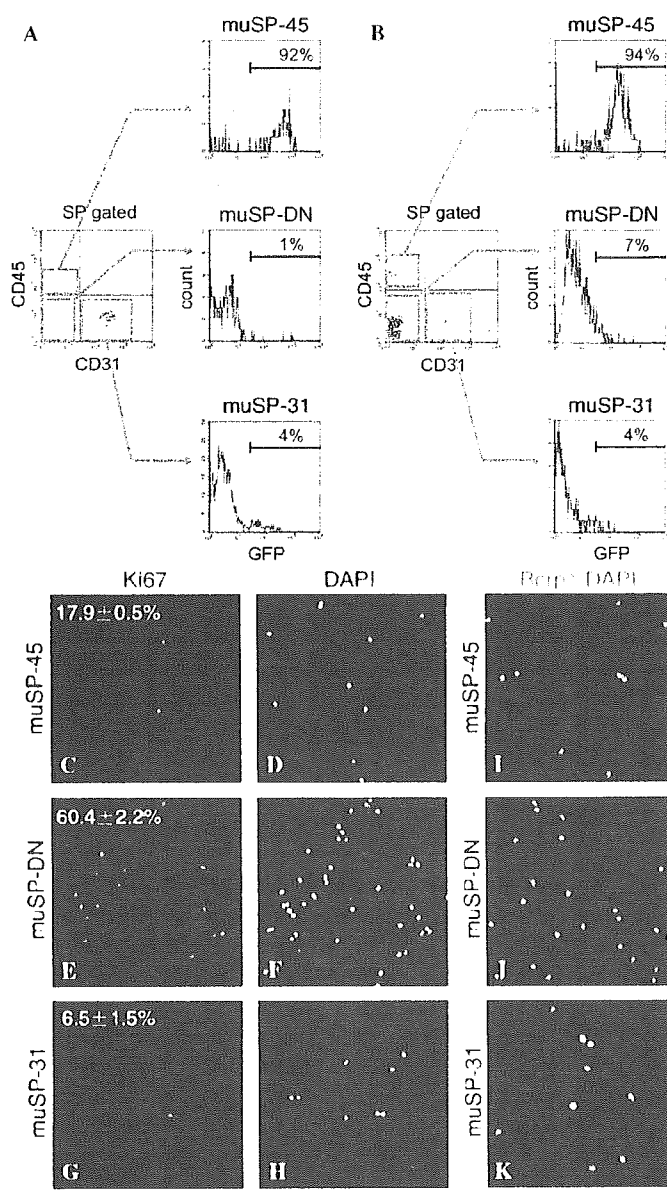


Fig. 3. Origin, proliferative activity, and Berp1 expression of subpopulations of muscle SP cells. (A,B) C57BL/6 mice were transplanted with whole BM from GFP⁺ Ig mice, and 3 months later, SP cells from untreated muscle (A) or regenerating muscle (3 days after CTX injection) (B) were further analyzed for CD31, CD45, and GFP expression. Note that CD45⁺ SP cells (middle and lower panels) are almost all negative for GFP, indicating that they do not originate from BM. In contrast, more than 90% of muSP-45 cells were GFP⁺ (upper panels). (C–H) Ki67 expression (green) and nuclei stained with DAPI (blue) on muSP-45 (C,D), muSP-DN (E,F), and muSP-31 (G,H) cells. The percentages of Ki67-positive cells were expressed as means ± SD of three independent experiments. muSP-45 (I), muSP-DN (J), and muSP-31 (K) were sorted from regenerating muscle and stained for Berp1 (green) and nuclei (blue). Only muSP-31 cells were stained positive for Berp1 (K). Bar: 50 μm.

myoblasts derived from satellite cells. muSP-DN cells from untreated muscle rapidly proliferated *in vitro* as observed in regenerating muscle (Fig. 2C). On the contrary, muSP-31 cells hardly expanded. After 2–3 weeks co-culture, both muSP-DN cells and muSP-31 cells differentiated not only into multinucleated myotubes co-expressing GFP and sarcomeric- α -actinin (Figs. 5E–G, only muSP-DN culture is shown) but also mononucleated myocytes (shown in insets). The frequency of mononucleated

myocytes was too low to quantify, but existence of these cells suggests that myogenic differentiation of SP cells could occur without fusion. Strikingly, the myotube-forming activity (the frequency of GFP⁺ myotubes, see Materials and methods for details) of muSP-DN cells was approximately 10-fold that of muSP-31 cells (Fig. 5H, lane for cont, 0.026 ± 0.007 vs 0.002 ± 0.001). In the experiments using SP cells from regenerating muscle at 3 days after CTX injection, muSP-DN cells showed the highest

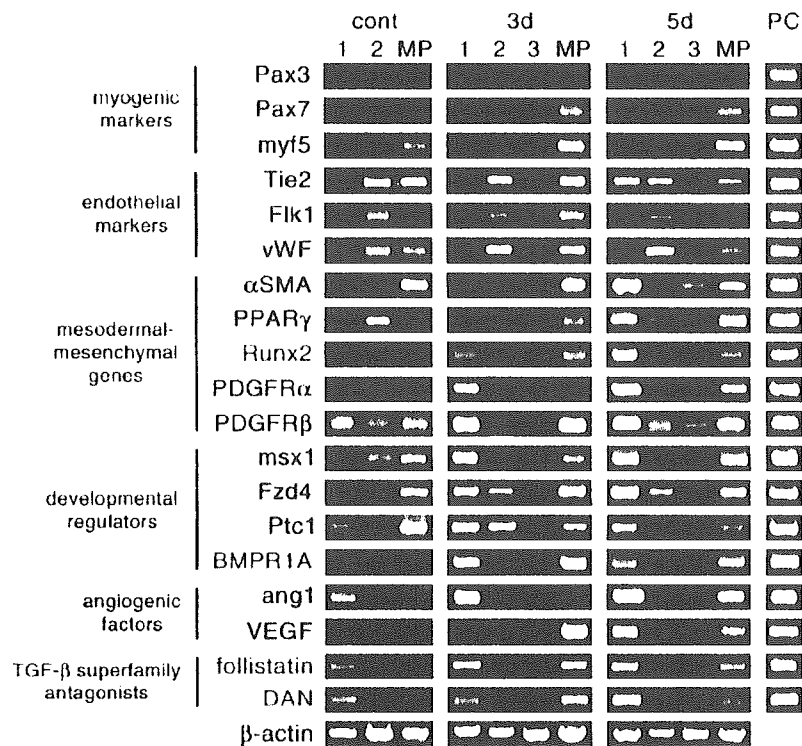


Fig. 4. Gene expression profiles of muscle SP cells during muscle regeneration. muSP-DN (lane 1), muSP-31 (lane 2), muSP-45 (lane 3), or MP cells were collected from untreated (cont) and regenerating muscle at 3 days (3d) or 5 days (5d) after CTX injection, and RT-PCR was performed against the indicated genes. Total embryo extract (E13) was used as a positive control (PC). β -actin was amplified to confirm that the quantities of mRNA were equal.

myotube-forming activity, although each SP subpopulation did form myotubes co-expressing GFP and sarcomeric- α -actinin (Fig. 5H, lane for CTX3d). This clearly demonstrates that muSP-DN cells have the highest myogenic potential among SP sub-fractions *in vitro*. For comparison, we quantified the myotube-forming activity of satellite cell-derived myoblasts. The value was 0.09 ± 0.01 , indicating that myogenic activity of myoblasts is much higher than that of muSP-DN cells.

Myogenic potential of muscle SP cells *in vivo*

To evaluate the myogenic potential of muscle SP cells *in vivo*, we performed transplantation experiments. muSP-DN or muSP-31 cells from untreated muscle of GFP Tg mice were directly transplanted into CTX-treated TA muscles of immunodeficient NOD/*scid* mice. Three weeks after transplantation, muSP-DN cells had generated myofibers more efficiently than muSP-31 cells (Figs. 6A and B, and Table 1), indicating that muSP-DN cells had relatively higher myogenic potential *in vivo* as well as *in vitro*. Contrary to our expectation, muSP-DN cells formed no GFP-positive adipocytes after transplantation.

Discussion

Muscle SP cells have been suggested to be multipotent and can contribute to skeletal muscle regeneration

[4,9,10,23]. However, most of these studies dealt with whole muscle SP cells as one functional unit. We subdivided, for the first time, muscle SP cells using CD31 and CD45 markers and revealed functional heterogeneity of muscle SP cells. CD31⁺CD45⁻ SP cells (muSP-31 cells) are a main subpopulation in non-regenerating muscle, but CD31⁻CD45⁻ SP cells (muSP-DN cells) which represent a minor subpopulation in non-regenerating muscle have the greatest differentiation potentials and become predominant subpopulation of SP cells upon muscle injury.

Differentiation potential of muscle SP cells

Phenotypic and immunohistochemical analysis suggested that muSP-31 cells are a subset of endothelial cells of capillaries and veins. They poorly proliferate after injury or in *in vitro* culture, and their differentiation potentials are limited both *in vitro* and *in vivo*.

CD45⁺ muscle SP cells (muSP-45 cells) were shown to have both hematopoietic and myogenic potentials, and hematopoietic potential of muscle-derived cells was exclusively found in this fraction [8,9]. We previously reported the contribution of muSP-45 cells to muscle regeneration [14]. In this study, we identified novel subpopulation that possesses much higher myogenic potential than muSP-45, muSP-DN.

muSP-DN cells showed the highest differentiation potential of all the mesenchymal lineages tested among

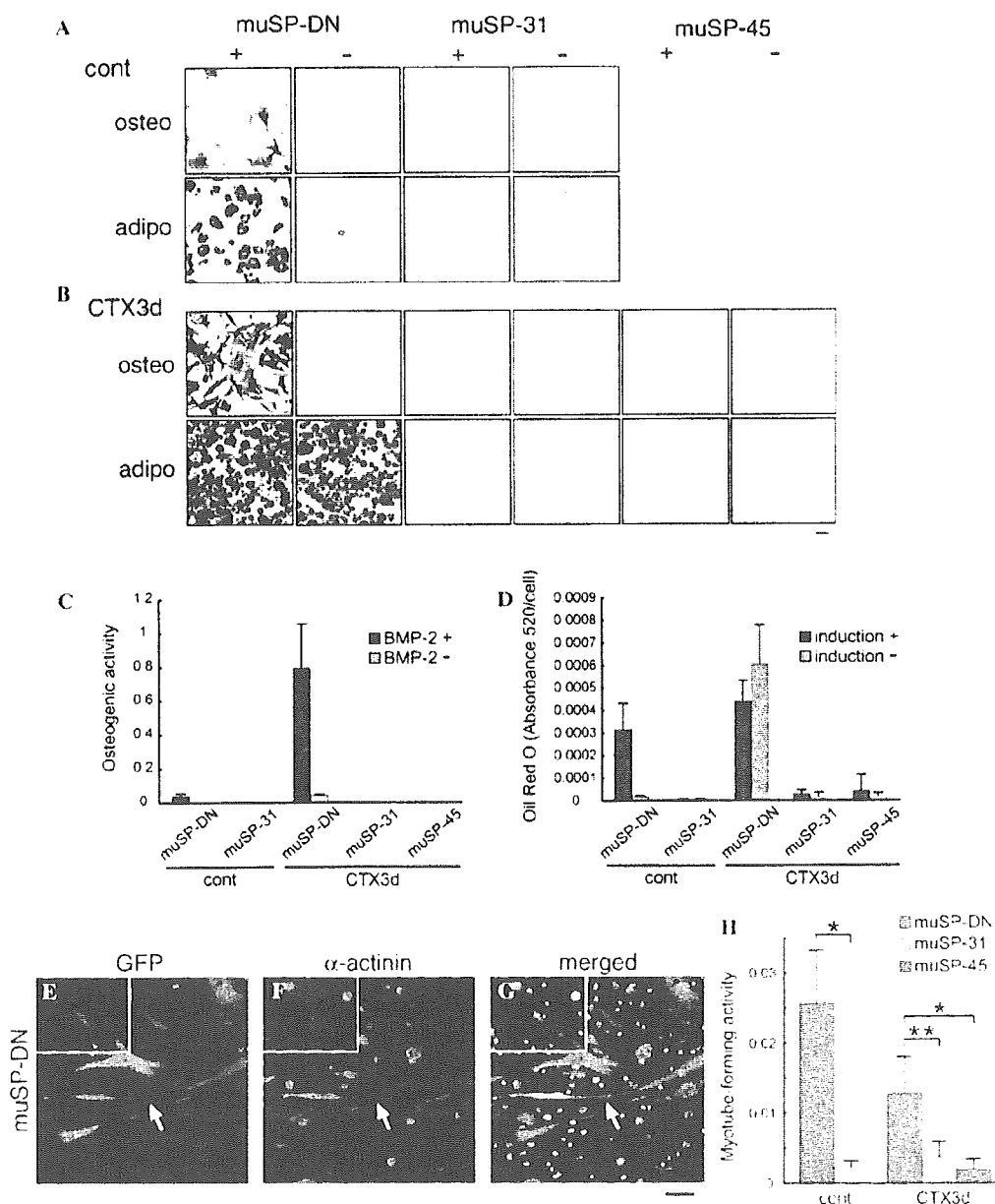


Fig. 5. muSP-DN cells differentiate into osteogenic cells, adipocytes, and skeletal muscle cells. (A,B) Three subpopulations of SP cells prepared from untreated (A) or regenerating (B) muscle were induced to differentiate into osteogenic or adipogenic cells. Uninduced cells (+) and induced cells (-) were then examined for alkaline phosphatase expression (osteo) or oil deposits (adipo). Bar: 50 μ m. (C,D) Osteogenic (C) and adipogenic (D) activities of subsets of SP cells prepared from control (cont) or regenerating muscle at 3 days after CTX injection (CTX3d) were quantified. Values are the average of three independent experiments. Error bars represent SD. (E-G) Co-culture of muscle SP cells with myoblasts. muSP-DN cells from GFP Tg mice were sorted and co-cultured with WT primary myoblasts in differentiation medium. Cells were stained with anti-GFP (green) and anti-sarcomeric α -actinin (red) antibodies. Nuclear staining with DAPI (blue) is shown in merged images (G). Insets show GFP⁺ mononucleated myocyte. Bar: 50 μ m. (H) Myotube-forming activities of muSP-DN cells (red bars), muSP-31 cells (blue bars), and muSP-45 cells (green bar) are shown. Each subpopulation was prepared from untreated (cont) or CTX-treated regenerating muscle (CTX3d). Values are the average of three independent experiments. Error bars represent SD. **P* < 0.01, ***P* < 0.05.

SP subpopulations. They were negative for lineage-specific markers under the non-regenerating condition, but after muscle injury or in in vitro expansion, they actively proliferated and were readily induced to express several mesenchymal genes. Their differentiation potential seems to be restricted to mesenchymal lineages because we did not

detect hematopoietic colonies derived from muSP-DN cells in vitro and muSP-DN cells failed to rescue the lethally irradiated mice (data not shown). These observations indicate that muSP-DN cells are enriched for primitive mesenchymal cells. This notion is further supported by gene expression pattern of muSP-DN cells. muSP-DN cells

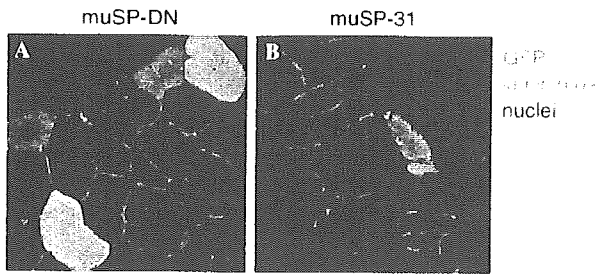


Fig. 6. muSP-DN cells participate in myofiber formation during muscle regeneration. (A,B) muSP-DN (A), muSP-31 (B) were transplanted into CTX-injected NOD/*Scid* muscles. Each subpopulation was prepared from untreated muscle of GFP Tg mice. Muscle sections were stained with anti-GFP (green) and anti-laminin $\alpha 2$ (red) antibodies 3 weeks after transplantation. More GFP-positive myofibers were detected in muSP-DN-transplanted muscles (A) than in muscles transplanted with muSP-31 cells (B). Bar: 40 μ m.

specifically expressed *ang1* under the non-regenerating condition and during the early phase of regeneration (Fig. 4, lane 1, cont or 3d). Perivascular cells, such as pericytes, express *ang1* [24,25], and several groups suggest that multipotent mesenchymal stem cells may be derived from pericytes [26–28]. A recent report demonstrated that vascular mural precursor cells are negative for endothelial markers but positive for *Tie2* and smooth muscle cell markers [29]. Likewise, muSP-DN cells were negative for *Flk1* and *eHf* throughout the regeneration process (Fig. 4, lane 1), but began to express *Tie2* and *α SMA* during late phases of regeneration (Fig. 4, lane 1, 5d). Given the similarity between muSP-DN cells and those reported perivascular primitive cells, muSP-DN cells would represent perivascular primitive mesenchymal cells in skeletal muscle.

Roles of muscle SP cells in muscle regeneration

muSP-DN cells actively proliferated and significantly increased in number upon muscle injury. The precise fate of muSP-DN cells has remained to be determined, since the number of muSP-DN cells returned to normal level at late stage of muscle regeneration.

We noted that angiogenic factors and TGF- β superfamily antagonists were strongly expressed in muSP-DN cells during muscle regeneration. Previous reports showed that *Ptc1*⁺ interstitial mesenchymal cells in muscle produce angiogenic factors, including *ang1*, and promote muscle regeneration after ischemia [30,31]. Some members of the TGF- β superfamily, such as myostatin and TGF- $\beta 1$, are known to act as negative regulators of myogenesis [32,33]. Inversely, one of the TGF- β superfamily antagonists, follistatin, has been reported to promote myoblast recruitment and fusion [34]. Therefore, muSP-DN cells might promote muscle regeneration by producing regeneration-regulating factors.

muSP-DN cells preferentially differentiate into myogenic cells after intramuscular transplantation, implying that normal muscle environment facilitates myogenic differenti-

ation of muSP-DN cells. However, we revealed that muSP-DN cells have a high tendency to differentiate into osteogenic or adipogenic cells in vitro. Therefore, it is possible that muSP-DN cells differentiate into osteogenic or adipogenic cells in some pathological conditions such as Duchenne muscular dystrophy [35,36]. Recent finding that microvascular pericytes can differentiate into adipocytes [37] further supports the notion that muSP-DN cells might be implicated in pathological changes.

In conclusion, we identified novel subpopulation of muscle SP cells, CD31⁺ CD45⁻ SP cells, which possesses capacity of mesenchymal differentiation in vitro and reveals myogenic differentiation potential in vivo. Our findings might provide new insights that may well be useful in understanding adult skeletal muscle regeneration and in designing therapeutic strategies of muscular dystrophy.

Acknowledgments

The authors are grateful to Ms. A. Fukase for technical assistance, and colleagues in Department of Molecular Therapy, especially Dr. M. Imamura, for useful discussion and suggestions on this work. This work is supported by Grants-in-Aid for Center of Excellence (COE), Research on Nervous and Mental Disorders (13B-1, 16B-2), and Health Science Research Grants for Research on the Human Genome and Gene Therapy (H13-genome-001, H16-genome-003), for Research on Brain Science (H12-Brain-025, H15-Brain-021) from the Ministry of Health, Labor and Welfare, Grants-in-Aids for Scientific Research (14657158, 15390281, and 16590333) from the Ministry of Education, Culture, Sports, Science and Technology, and a Research Grant from National Space Development Agency of Japan (NASDA) and the Japan Space Forum.

Appendix A. Supplementary data

Supplementary data associated with this article can be found, in the online version, at doi:10.1016/j.bbrc.2006.01.037.

References

- [1] R. Bischoff, Satellite and stem cells in muscle regeneration, in: A.G. Engel, C. Franzini-Armstrong (Eds.), *Myology*, McGraw-Hill, New York, 2004, pp. 66–86.
- [2] G. Ferrari, G. Cusella-De Angelis, M. Coletta, E. Paolucci, A. Stornaiuolo, G. Cossu, F. Mavilio, Muscle regeneration by bone marrow-derived myogenic progenitors, *Science* 279 (1998) 1528–1530.
- [3] M.A. Goodell, K. Brose, G. Paradis, A.S. Conner, R.C. Mulligan, Isolation and functional properties of murine hematopoietic stem cells that are replicating in vivo, *J. Exp. Med.* 183 (1996) 1797–1806.
- [4] E. Gussoni, Y. Soneoka, C.D. Strickland, E.A. Buzney, M.K. Khan, A.F. Flint, L.M. Kunkel, R.C. Mulligan, Dystrophin expression in the mdx mouse restored by stem cell transplantation, *Nature* 401 (1999) 390–394.
- [5] S. Fukada, Y. Miyagoe-Suzuki, H. Tsukahara, K. Yuasa, S. Higuchi, S. Ono, K. Tsujikawa, S. Takeda, H. Yamamoto, Muscle regener-